Check for updates

A ring-fluorinated heptamethine cyanine dye: synthesis, photophysical properties, and vapochromic properties in response to ammonia†

Shouhei Ajioka,[a] Yuto Hagiyama,[a] Yuki Uehashi,[a] Tomohiro Agou, [iD][b] Yasuhiro Kubota,[a] Toshiyasu Inuzuka[c] and Kazumasa Funabiki [iD] *[a]

Heptamethine cyanine dyes (HMCDs) have attracted considerable attention in biological and energy applications owing to their unique near-infrared (NIR) photophysical properties. Therefore, the development of molecules that change both visible and fluorescent colours in a stimulus-responsive manner by exploiting the NIR optical properties of HMCDs has been a subject of increasing interest. Most research results are based on a highly nucleophilic anion addition or reversible *intramolecular* addition reaction of a *weakly nucleophilic neutral nucleophile* with the C=N bond of the terminal indol-1-ium moiety. Examples of *intermolecular* addition of weakly neutral nucleophiles and the use of solid or polymer materials are not available. Here, we report the synthesis of a NIR-absorbing ring-perfluorinated HMCD. The HMCD's unique properties in various solvents and rapid and reversible vapochromic response to various amines, including NH_3, based on the noteworthy structural modification induced by fluorine atoms on the aromatic ring are also presented. The ring-fluorinated HMCD adsorbed on neutral filter paper responds quickly to even low-nucleophilicity NH_3 vapour. Repeatability tests on filter paper adsorbed with the ring-fluorinated HMCD and NH_3 and HCl vapours show excellent reproducibility in 13 blue-green and yellow colour transitions. These results are the first examples of intermolecular addition of weakly neutral nucleophiles into HMCDs and stimulus responsiveness not in solutions.

Introduction

Polymethine cyanine dyes having azaheterocycles at both ends of the polymethine backbone offer advantages such as narrow absorption bands, high absorption coefficients, and readily tunable maximum absorption wavelengths (λ_{abs}) and maximum fluorescence wavelengths (λ_{em}) within the visible and near-infrared (NIR) regions.[1] In particular, heptamethine cyanine dyes (HMCDs), which exhibit absorption and fluorescence emissions in the NIR region, are attracting considerable attention as one of the most promising molecules for photo-science and -technology using NIR light, such as imaging,[2] therapy,[3] and organic solar cells.[4,5]

The development of molecules that change both the colours of the solutions or films and fluorescent colours in a stimulus-responsive manner by exploiting the NIR optical properties of HMCDs has been a subject of increasing interest. Changing both the colours of the solutions and fluorescent colours of the HMCD reported thus far is mostly based on (1) highly nucleophilic anion addition, such as cyanide anion (CN^-), to the C=N bond of the terminal indol-1-ium moiety (Fig. 1(a))[6] or (2) a reversible *intramolecular* addition reaction of *weakly nucleophilic neutral nucleophiles*, such as nitrogen, sulfur, and oxygen atoms, with the C=N bond of the indol-1-ium moiety or the C=C double bond at the meso position, depending on the pH of the solution (Fig. 1(b)).[7] However, *intermolecular* addition of weakly neutral nucleophiles is not reported. In addition, all HMCDs were in solution, and no examples of the use of solid or polymer materials are available.

Ammonia (NH_3) is currently attracting attention as a fuel that can replace oil, coal, and natural gas for power generation because it does not emit carbon dioxide when burned. Ammonia is expected to be an energy carrier for the transport and storage of hydrogen.[8] Although many studies on the vapochromism of organic dyes or metal complexes towards NH_3 have been reported,[9] to the best of our knowledge, only one study has been conducted on the reversible vapochromic responsiveness of HMCDs adsorbed on silica gels to various amines, as shown in

[a] Department of Chemistry and Biomolecular Science, Gifu University, 1-1 Yanagido, Gifu 501-1193, Japan. E-mail: funabiki.kazumasa.m6@f.gifu-u.ac.jp

[b] Department of Material Science, Graduate School of Science, University of Hyogo, 3-2-1 Koto, Kamigori-cho, Ako, Hyogo 678-1297, Japan

[c] Division of Instrumental Analysis, Life Science Research Center, Gifu University, 1-1 Yanagido, Gifu 501-1193, Japan

† Electronic supplementary information (ESI) available. CCDC 1987380 and 1987381. For ESI and crystallographic data in CIF or other electronic format see DOI: https://doi.org/10.1039/d4ma00962b
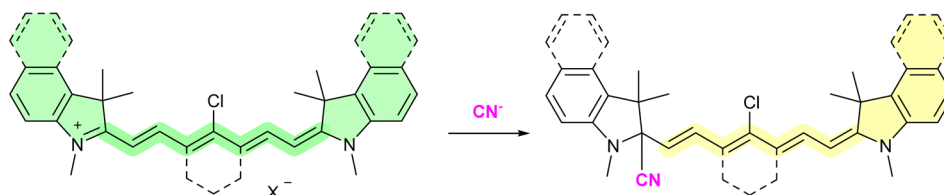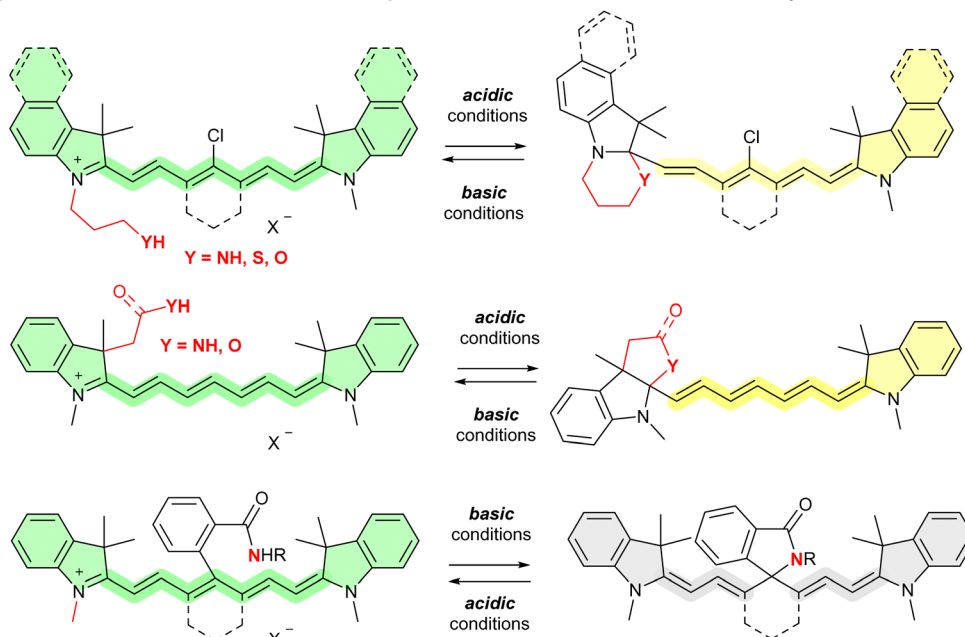
(a) Addition of a highly nucleophilic *cyanide anion (CN⁻)* to the *C=N bond* of the indolenium moiety

(b) *Intramolecular* addition of the *neutral* nucleophiles to the *C=N bond* of the indolenium moiety

Fig. 1 Previous methods for changing the colour or fluorescence of HMCDs in solutions by intermolecular addition of cyanide anion (a) or intramolecular addition of neutral nucleophiles (b).

Fig. 2.[10] The results revealed that the vapochromism due to the intermolecular addition of weakly nucleophilic neutral amines to the HMCD can be attributed to the adsorption of the dye on weakly acidic silica gel. However, the NH_3 vapour of the HMCD adsorbed on the weakly acidic silica gel was insufficient because NH_3 is not sufficiently nucleophilic.

The unique functions of organic dyes can be incorporated by introducing heteroatoms such as sulfur,[11] phosphorous,[12] and silicon[13] into the electron-conjugated system or on the aromatic rings of the functional dyes. The functional dyes carrying partially ring-fluorinated aromatics or heteroaromatics have garnered attention as fluorescent dyes,[14] organic field-effect transistors,[15] organic photovoltaic cells,[16] and amine-response dyes[17] owing to their excellent properties, including their atomic size that is almost as small as that of a hydrogen atom, their highest electronegativity, their strong carbon–fluorine bond energy, and some interactions with other elements.[18] However, only limited examples of stimulus-responsive NIR-absorbing molecules or materials carrying ring-fluorinated aromatics or heteroaromatics are available.[19] Although only a
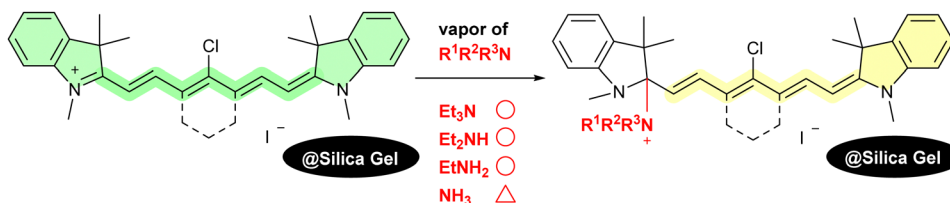
Intermolecular* addition of the *amines* to the *C=N bond* of the indolenium moiety of HMCD *adsorbed on silica gel

Fig. 2 Previous method for changing the colour of HMCD towards vapour of amines.

few patents on the preparation of ring-fluorinated HMCDs exist, the structure and optical and other properties of such HMCDs have not yet been reported.[20] Here, we report (1) the synthesis of a NIR-absorbing ring-perfluorinated HMCD and its (2) crystal structure, (3) unique properties in various solvents, and (4) rapid and reversible vapochromic response to various amines including NH_3, based on the noteworthy structural modification induced by fluorine atoms on the aromatic ring. The results reveal the first examples of intermolecular addition of weakly neutral nucleophiles to HMCD and stimulus responsiveness not in solutions.

Results and discussion

Synthesis

As shown in Scheme 1 (eqn (1), successive treatment of a commercially available 2,3,4,5-tetrafluoroaniline with sodium nitrite in water at −10 °C and tin chloride(II) hydrate at room temperature in the presence of concentrated hydrochloric acid yields 2,3,4,5-tetrafluorophenyl hydrazine hydrochloride. The obtained crude hydrazine hydrochloride reacts with 3-methyl-2-butanone in acetic acid at 120 °C in the presence of sodium acetate and results in the formation of 4,5,6,7-tetrafluoro-2,3,3-trimethyl-3H-indole (1) in 22% yield from 2,3,4,5-tetrafluoroaniline.

The reaction between 1 and an excess amount of the most reactive haloalkane, iodomethane, does not proceed because

the nucleophilicity of 1 is significantly reduced owing to the strong electron-withdrawing property of the fluorine atom. Treatment of 1 with 2 equiv. of the Meerwein reagent (trimethyloxonium tetrafluoroborate) in chloroform for 24 h under reflux results in the formation of 4,5,6,7-tetrafluoro-1,2,3,3-tetramethyl-3H-indol-1-ium tetrafluoroborate (2a) in 84% yield. The tetrafluoroindolium salt (2a) smoothly reacts with dialdehyde (3) in dimethylformamide (DMF) even at 23 °C, which is a very low temperature compared with a typical reaction temperature (120 °C), for 18 h and results in the formation of 2-((E)-2-((E)-2-chloro-3-(2-((E)-4,5,6,7-tetrafluoro-1,3,3-trimethylindolin-2-ylidene)ethylidene)cyclohex-1-en-1-yl)vinyl)-4,5,6,7-tetrafluoro-1,3,3-trimethyl-3H-indol-1-ium tetrafluoroborate (4a) in 84% yield (Scheme 1, eqn (2)).[21] The reaction of a fluorine-free indolium salt (2b) with 3 in DMF under the same reaction conditions (at 23 °C for 18 h) results in the formation of 2-((E)-2-((E)-2-chloro-3-(2-((E)-1,3,3-trimethylindolin-2-ylidene)ethylidene)cyclohex-1-en-1-yl)vinyl)-1,3,3-trimethyl-3H-indol-1-ium tetrafluoroborate (4b) with only 9% yield, together with a 20% yield of (E)-2-chloro-3-(2-((E)-1,3,3-trimethylindolin-2-ylidene)ethylidene)cyclohex-1-ene-1-carbaldehyde (5b) (Scheme 1, eqn (3)). The high-temperature (120 °C) conditions allow the reaction of 2b with 3 in DMF to proceed smoothly for 3 h, giving a satisfactory yield (76%) of nonfluorinated HMCD (4b). These results may be attributed to an increase in the acidity of the hydrogen atom on the methyl group at the 2-position of 2a owing to the strong
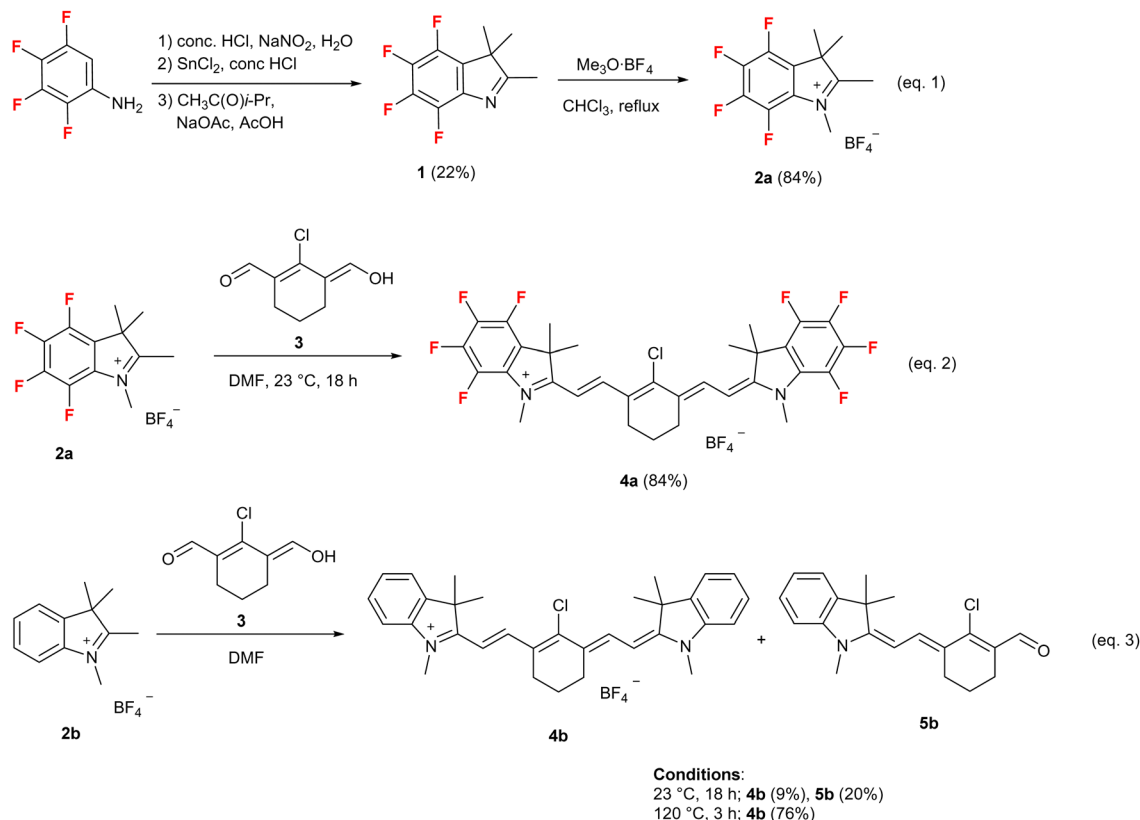
Scheme 1 Preparation of the ring-fluorinated and non-fluorinated HMCDs (**4a** and **4b**, respectively).

electron-withdrawing property of the four fluorine atoms on the aromatic ring. Consequently, the formation of the enamine from **2a** and successive condensation with **3** occur smoothly, *even at room temperature* to result in the formation of the corresponding ring-fluorinated HMCD (**4a**) in good yield.

Single-crystal structural analysis

Single crystals of **4a** and **4b** were prepared using the vapour diffusion method with dichloromethane (DCM) and hexane. Single-crystal X-ray analysis results of the obtained HMCDs (**4a**: CCDC No. 1987380, monoclinic, $P2_1/c$ space group; **4b**: CCDC No. 1987381, orthorhombic, $Pca2_1$ space group) are shown in Fig. 3 and 4.

The twist and fold angles of the two indolium planes of HMCD **4b**[21] or the two ring-fluorinated indolium planes of HMCD **4a** were measured by using the Olex2 software[22] and are shown in Fig. 3(a) and 4(a). The twist angle between the two ring-fluorinated indolium planes of HMCD **4a** is 45.25°, which is considerably larger than that (17.99°) between the two non-fluorinated indolium planes of HMCD **4b**. These results are consistent with those of the ring-fluorinated trimethine cyanine dye.[23] The fold angle between the two ring-fluorinated indolium planes of HCMD **4a** is 0.38°, which is smaller than that (4.82°) between the non-fluorinated indolium planes of HMCD **4b**. These results are not consistent with those of the ring-fluorinated trimethine cyanine dye.[23] As shown in Fig. 4(b) and (c), compared with the ring-fluorinated HMCD **4a**, in the structure of HMCD **4b**, less intramolecular and intermolecular interactions occur between the fluorine atom and other atoms. By contrast, ring-fluorinated HMCD **4a** exhibits six types of intramolecular interactions between fluorine atoms and other atoms, such as hydrogen, chlorine, and carbon atoms (Fig. 3(b)), and four types of intermolecular interactions between fluorine atoms and hydrogen, carbon, and nitrogen atoms (Fig. 3(c)). The packing of the molecules observed in the single-crystal X-ray analysis of HMCDs **4a** and **4b** is shown in Fig. S1 and S2 (ESI†). Molecular orientations are indicated with four colors: red, blue, magenta, and green, in both HMCDs. As shown in Fig. S1(a) (ESI†), in the case of ring-perfluorinated HMCD **4a**, both the blue and magenta molecules and the red and green molecules are arranged in the same direction. In addition, the blue and magenta molecular arrangements and the red and green molecular arrangements are opposite. As shown in Fig. S1(g), (h), (i), and (j) (ESI†), the distances between the indolium ring and the methine double bond are 4.988, 5.091, and 6.439 Å, and the distance between the two indolium rings is ~5.5 Å. No π–π stacking is observed. As shown in Fig. S2 (ESI†), in the case of fluorine-free HMCD **4b**, the blue and magenta molecules and the red and green molecules are arranged in a herringbone shape. The distances between the indolium ring and the methine double bond are 4.274 and 5.918 Å, as depicted in Fig. S2(b) and (f) (ESI†). No π–π stacking is observed.

Ultraviolet-visible (UV-vis)-NIR absorption and fluorescence spectra and behaviour in various solvents

The UV-vis-NIR absorption (solid line) and fluorescence (dotted line) spectra of HMCDs **4a** and **4b** in DCM (1×10^{-6} M) are shown in Fig. 5.
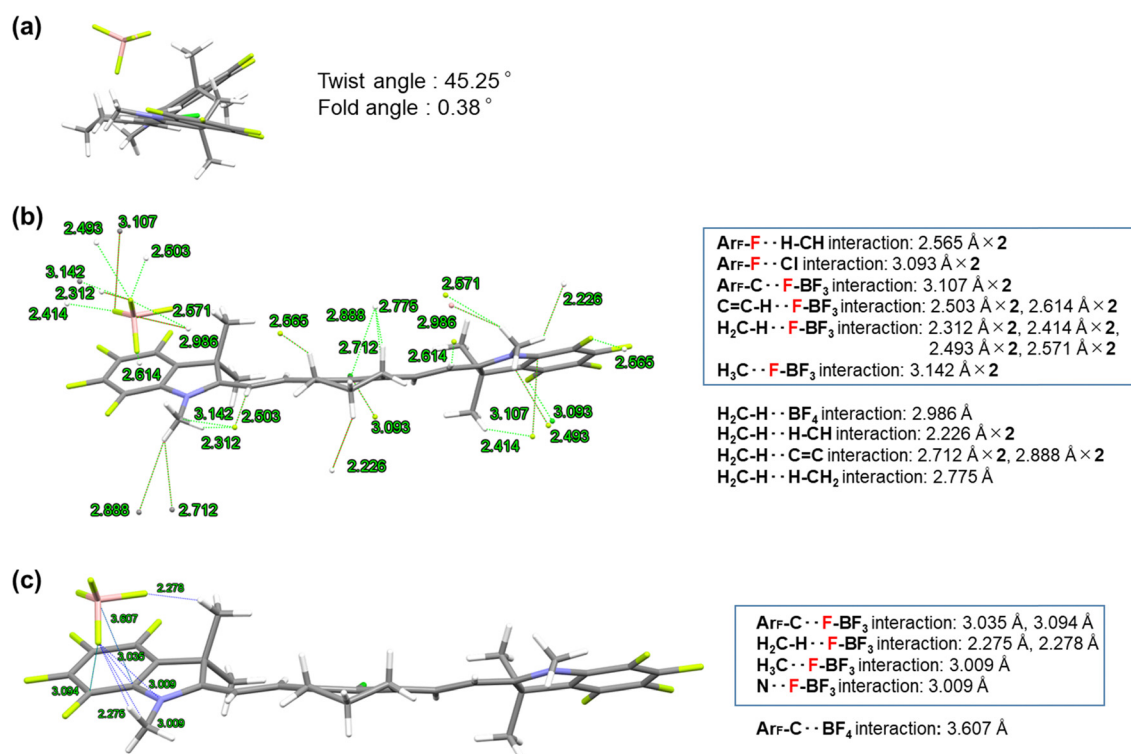

Fig. 3 X-ray diffraction structures of HMCD **4a**: twist and fold angles (a), intermolecular short contacts (b), and intramolecular short contacts (c).
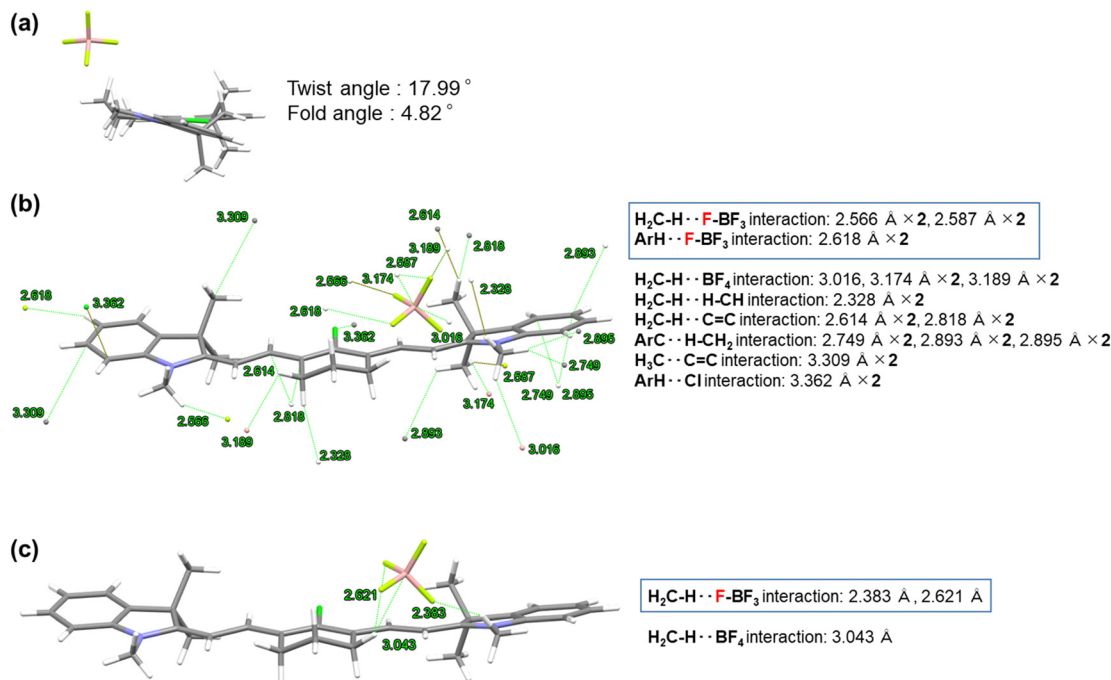
Fig. 4 X-ray diffraction structures of the ring-fluorinated HMCD (**4b**): twist and fold angles (a), intermolecular short contacts (b), and intramolecular short contacts (c).
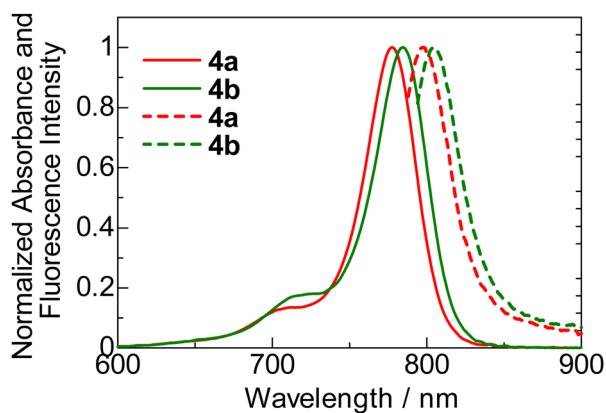

Fig. 5 Normalised UV-vis-NIR absorption (solid line) and fluorescence (dotted line) spectra of HMCDs **4a** and **4b** in DCM (1×10^{-6} M).

The λ_{abs} values of **4a** and **4b** in DCM are within the NIR region (778 and 785 nm, respectively). The λ_{abs} value of ring-fluorinated HMCD **4a** is 7 nm blue-shifted compared with that of non-fluorinated HMCD **4b**. The molar absorption coefficients (ε) of **4a** and **4b** are 318 000 and 331 000, respectively. Similar to λ_{abs}, λ_{em} of ring-fluorinated HMCD **4a** is 5 nm blue-

shifted compared with that of non-fluorinated HMCD **4b**. The Stokes shifts (SS) of HMCDs **4a** and **4b** are small (322 and 301 cm^{-1}, respectively). The fluorescence quantum yields ($\varPhi_f$) of both HMCDs are low, and the τ_f of ring-fluorinated HMCD **4a** is slightly smaller than that of non-fluorinated HMCD **4b**. The fluorescence lifetime (τ_s) of ring-fluorinated HMCD **4a** is slightly shorter than that of non-fluorinated HMCD **4b**. These results may be attributed to ring-fluorinated HMCD **4a** having a higher non-radiative rate constant than non-fluorinated HMCD **4b** (Table 1).

The UV-vis-NIR absorption and fluorescence spectra of non-fluorinated HMCD **4b** in various solvents, such as methanol (MeOH), ethanol (EtOH), 2-propanol (i-PrOH), acetonitrile (MeCN), and acetone, were recorded after preparing the solution and leaving it at room temperature for 3 h. The spectra and images are shown in Fig. 6 and summarised in Table 2. Similar to previous results with other anions,[22] λ_{abs} (774–785 nm) and λ_{em} (795–804 nm) are in the NIR region, and negative solvatochromism is observed in the UV-vis-NIR and fluorescence spectra.

By contrast, ring-fluorinated HMCD **4a** exhibits unique properties in various solvents. The spectra and photographs in various solvents are shown in Fig. 7 and summarised in

Table 1 Absorption maximum (λ_{abs}), molar absorption coefficient (ε), and fluorescence properties of HMCDs **4a** and **4b** in DCM

Dye	$\lambda_{abs}{}^{a}$ (nm)	ε^{a} (M^{-1} cm^{-1})	$\lambda_{em}{}^{a}$ (nm)	SS (cm^{-1})	$\varPhi_f{}^{b}$	$\tau_s{}^{c}$ (ns)	$k_f{}^{d}$ (10^9 s^{-1})	$k_{nr}{}^{e}$ (10^9 s^{-1})
4a	778	318 000	798	322	0.11	0.9	0.13	1.01
4b	785	331 000	804	301	0.14	1.3	0.13	0.77

[a] Measured in DCM (1×10^{-6} M). [b] Measured using an integrating sphere method. [c] Measured using a single-photon-counting method. [d] Radiative rate constant ($k_f = \varPhi_f/\tau_s$). [e] Non-radiative rate constant ($k_{nr} = (1 - \varPhi_f)\tau_s$).
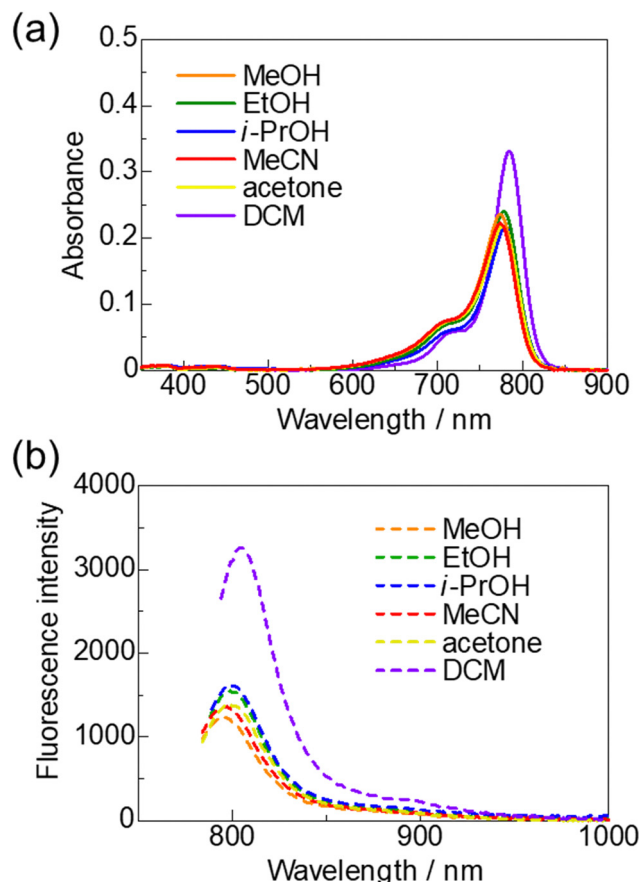
Fig. 6 UV-vis-NIR absorption spectra (a) and fluorescence spectra (b) of non-fluorinated HMCD **4b** in various solvents (1×10^{-6} M).

Table 2 Absorption maximum and molar absorption coefficients of HMCDs **4a** and **4b** in various solvents (1×10^{-6} M)

Dye	Solvent	$\lambda_{abs}{}^{a}$ (nm)	ε^{a} (M^{-1} cm^{-1})
4a	MeOH	400	49 000
	EtOH	402	46 000
	i-PrOH	399	39 000
	MeCN	404, 770	32 000, 103 000
	Acetone	406, 773	46 000, 15 000
	DCM	778	318 000
4b	MeOH	774	235 000
	EtOH	778	239 000
	i-PrOH	779	216 000
	MeCN	774	222 000
	Acetone	774	218 000
	DCM	785	331 000

[a] Measured in solvents (1×10^{-6} M).

Table 2. The peaks at approximately 774–779 nm disappear in the case of MeOH and EtOH, and a new peak appears at approximately 400 nm (Fig. 7(a)). As displayed in Fig. 7(b), the peaks around 774–779 nm are small in the case of i-PrOH, MeCN, and acetone. Furthermore, as shown in Fig. 7(d), fluorescence spectra of ring-fluorinated HMCD **4a** excited at λ_{abs} (770–778 nm) in DCM, MeCN, and acetone are observed at 790–798 nm. However, note that no fluorescence spectrum

exists at λ_{abs} (399–406 nm) in the case of MeOH, EtOH, i-PrOH, MeCN, and acetone.

Electrochemical and thermal properties

Thermogravimetry-differential thermal analysis (TG-DTA) was performed to determine the decomposition temperatures (T_{dt}) of HMCDs **4a** and **4b**. The results of T_{dt} are shown in Fig. S3 (ESI†) and listed in Table 3. Ring-perfluorinated HMCD **4a** shows a lower T_{dt} (238.0 °C) than non-fluorinated HMCD **4b** (244.9 °C).

HMCDs **4a** and **4b** undergo oxidation at 0.693 and 0.478 V (*versus* the saturated calomel electrode (SCE)) in the cyclic voltammograms, respectively, as shown in Fig. S6 (ESI†). The E_{HOMO} values for HMCDs **4a** and **4b** were calculated using the values of E_{ox} in the cyclic voltammograms, and the E_{LUMO} values for HMCDs **4a** and **4b** were obtained by performing calculations using the E_{HOMO} values and the bandgap values, which can be obtained from the onset of the absorption spectra. The highest occupied molecular orbital (HOMO) and the lowest unoccupied molecular orbital (LUMO) energies of aromatic ring-perfluorinated HMCD **4a** were much lower than those of non-fluorinated HMCD **4b** because of the high electronegativity of the fluorine atom.

Density functional theory (DFT) calculations

DFT calculations in the gas phase were performed at the B3LYP/6-31G(d,p) level with Gaussian 16 for HMCDs **4a** and **4b** performed to examine the electronic states of the HOMO and LUMO levels and bandgaps, and the results are illustrated in Fig. 8. Although a significant difference in the electron distribution between the HOMO and LUMO in HMCDs **4a** and **4b** is unlikely, the introduction of fluorine atoms into the aromatic ring of the dye lowers the levels of the HOMO and LUMO, especially the HOMO. Therefore, the bandgap of ring-fluorinated HMCD **4a** is wider than that of non-fluorinated HMCD **4b**. These results support that the λ_{abs} (778 nm) of ring-fluorinated HMCD **4a** is blue-shifted compared with that of non-fluorinated HMCD **4b** (785 nm).

Photostability

As presented in Fig. 9(a)–(c), the photostabilities of ring-fluorinated HMCD **4a** and non-fluorinated HMCD **4b** in an incubator at 25 °C under white-light-emitting diode (LED) irradiation (8.5 W) are measured in CH_2Cl_2 solutions (1.0×10^{-6} M). The results for the condition when the HMCDs are left in the dark without LED irradiation in CH_2Cl_2 are depicted in Fig. 9(d). CH_2Cl_2 is used as the solvent because the lifetime of singlet oxygen is longer in CH_2Cl_2 than in other solvents, such as alcohols, benzene, and alkanes. The residual rates of HMCD **2a** and **2b** are calculated from the changes at λ_{abs} in the UV-vis-NIR absorption spectra.

After 6 days of light irradiation, the residual rates of HMCDs **4a** and **4b** in CH_2Cl_2 are 92% and 78%, respectively (Fig. 9(c)). The photostability of ring-fluorinated HMCD **4a** is higher than that of **2b**. Non-fluorinated HMCD **4b** in the CH_2Cl_2 solution kept in the dark does not degrade at all, and its residual rate is
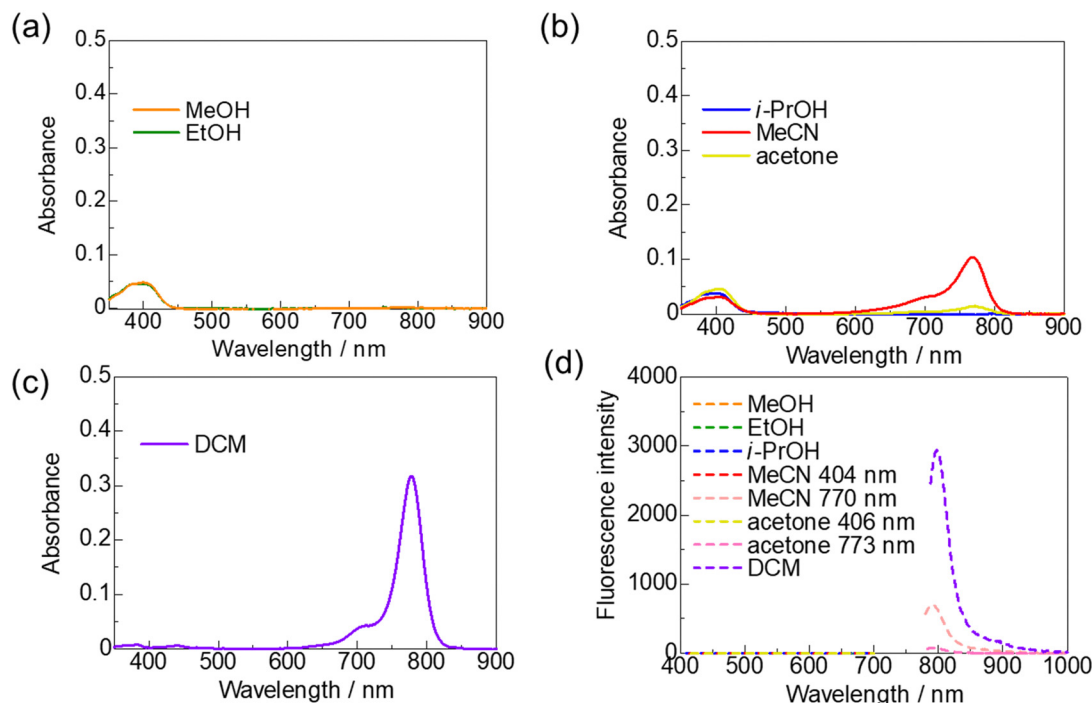
Fig. 7 UV-vis-NIR absorption spectra in MeOH and EtOH (a), in i-PrOH, MeCN, and acetone (b), and in DCM (c). Fluorescence spectra (d) of ring-fluorinated HMCD **4a** in various solvents (1×10^{-6} M).

Table 3 T_{dt} and electrochemical properties of HMCDs **4a** and **4b**

Dye	$T_{dt}{}^a$ (°C)	$E_{ox}{}^b$ (V vs. SCE)	HOMO^c (eV)	$\lambda_{onset}{}^d$ (nm)	HOMO–LUMO gap^e (eV)	LUMO^f (eV)
4a	238.0	0.693	−5.09	875	1.42	−3.67
4b	244.9	0.478	−4.88	883	1.41	−3.47

^{a} Decomposition temperatures (T_{dt}) were determined by conducting TG-DTA. ^{b} Measured in MeCN containing the dyes (1×10^{-3} M) and Bu$_4$NClO$_4$ (0.1 M) and recalculated as E_{ox} (V vs. SCE). ^{c} HOMO (eV) = − (E_{ox} (V vs. SCE) + 4.4). ^{d} Measured in CH$_2$Cl$_2$ (1×10^{-6} M). ^{e} HOMO–LUMO gap (eV) = $1240/\lambda_{onset}{}^{abs}$ (nm). ^{f} LUMO (eV) = HOMO − (HOMO–LUMO gap).

99%. These results indicate that the introduction of a strong electron-withdrawing fluorine atom into the indolenine portion of HMCD stabilises the HOMO and the LUMO and reduces the electron density of the double bond, thus improving the photostability of the dye.[23]

Stimulus response to amines

Based on the interesting absorption properties of ring-fluorinated HMCD **4a** in various solvents, the stimulus responsiveness of ring-fluorinated HMCD **4a** to other neutral nucleophiles such as triethylamine (TEA) in solutions was evaluated, as shown in Fig. 10.

Various amounts (10, 20, 30, 40, 50, 100, 200, and 300 equiv.) of TEA were added to a highly concentrated DCM solution (5×10^{-6} M) of HMCDs **4a** and **4b** at room temperature, and UV-vis-NIR spectra were recorded after the solution was prepared and left at room temperature for 4 h, as presented in Fig. 10 and Table 4.

The results of the UV-vis-NIR spectra and the photographs obtained under white LED irradiation are shown in Fig. 10.

Although the values (784–785 nm) of λ_{abs} in the DCM solution of non-fluorinated HMCD **4b** in the presence of various amounts of TEA are almost unchanged in the UV-vis-NIR spectra, the λ_{abs} of ring-fluorinated HMCD **4a** shifts from 778–782 nm to 409–416 nm, and the colour of the DCM solution of the HMCD **4a** changes from green to yellow (Fig. 10(c)). An excellent linear relationship between the absorption log (A_{409}/A_{778}) and the equiv. of TEA is observed, as shown in Fig. 10(f). Based on this linearity, the limit of detection (LOD) for **4a** is determined as LOD = $3s/k$, where s is the standard deviation (Fig. 10(e)) obtained from five measurements, and k is the slope of the line. The results indicate that the LOD of ring-fluorinated HMCD **4a** is 2.97×10^{-6} M.

^{1}H, ^{13}C, and ^{19}F nuclear magnetic resonance (NMR) spectra of ring-fluorinated HMCD **4a** in deuterochloroform (CDCl$_3$) without or with an excess amount of TEA were recorded to assess the structural changes in ring-fluorinated HMCD **4a** in a DCM solution. The results of not only ^{1}H, ^{19}F, and ^{13}C NMR spectroscopy of ring-fluorinated HMCD **4a** without or with an excess amount of TEA but also high-resolution mass
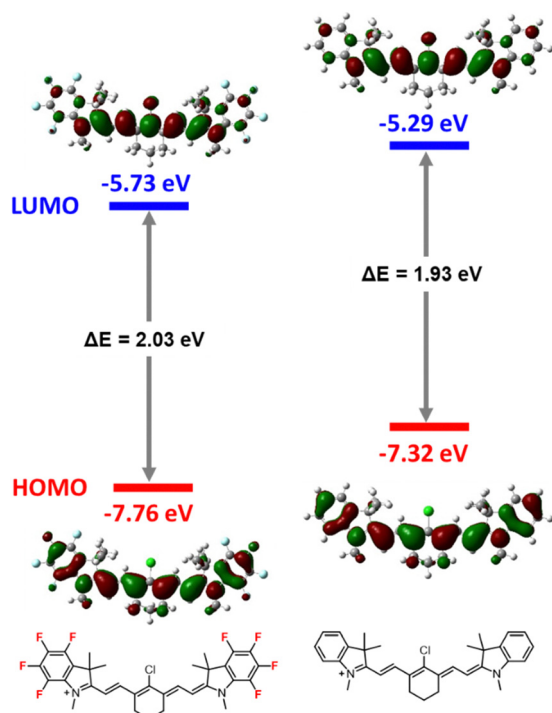
Fig. 8 Energy diagram and molecular orbitals of the cationic parts of HMCDs **4a** and **4b** calculated using DFT at the B3LYP/6–31G(d,p).

spectrometry (HRMS) are shown in Fig. 11. Two types of vinyl protons (H$_a$ and H$_b$) in ^{1}H NMR of **4a**, four types of aromatic

fluorine atoms in ^{19}F NMR, and four types of alkyl carbons and an imine carbon atom (173 ppm) (magenta-filled circles) in ^{13}C NMR are observed,[17b] because ring-fluorinated HMCD **4a** has a resonance structure, that is, a particular electronic structure arising from a symmetric, positively charged, amino-terminated, 7-numbered polymethine chain.

Because of the collapse of the symmetric resonance structure caused by the addition of TEA to aromatic ring-fluorinated HMCD **4a**, four types of vinyl protons, H$_a$, H$_a'$, H$_b$, and H$_b'$, appear in the ^{1}H NMR spectra, similar to our previously reported ^{1}H NMR spectra of ring-fluorinated trimethine cyanine dye with *n*-hexylamine added to the C=N bond.[17b] Eight types of aromatic fluorine atoms in the ^{19}F NMR spectra and nine types of alkyl carbons (orange-filled circles) in the ^{13}C NMR spectra are observed. The peak at 173.0 ppm corresponding to the iminium carbon disappears and shifts to 156.9 ppm in the ^{13}C NMR spectra. These results suggest that the addition of TEA to ring-fluorinated HMCD **4a** proceeds smoothly with CDCl$_3$ at room temperature to yield the corresponding TEA adduct with a molecular weight of 728.3011, as confirmed by performing HRMS with high-performance liquid chromatography (Fig. 11(d)).

Finally, the reversible vapochromic responses of the filter papers adsorbing ring-fluorinated HMCD **4a** and non-fluorinated HMCD **4b** to amine vapour were investigated. The filter papers adsorbing ring-fluorinated HMCD **4a** and non-fluorinated HMCD **4b** were prepared by soaking white filter papers in a DCM solution (5 × 10^{-4} M) of HMCDs **4a** and **4b**
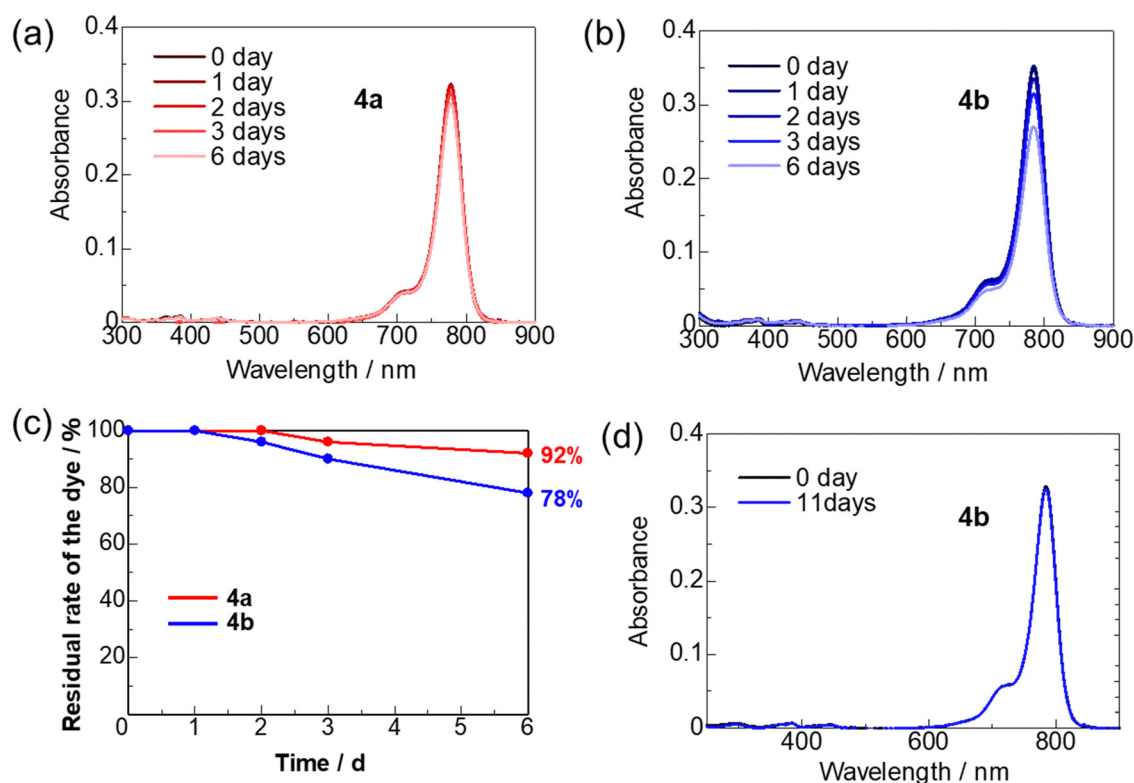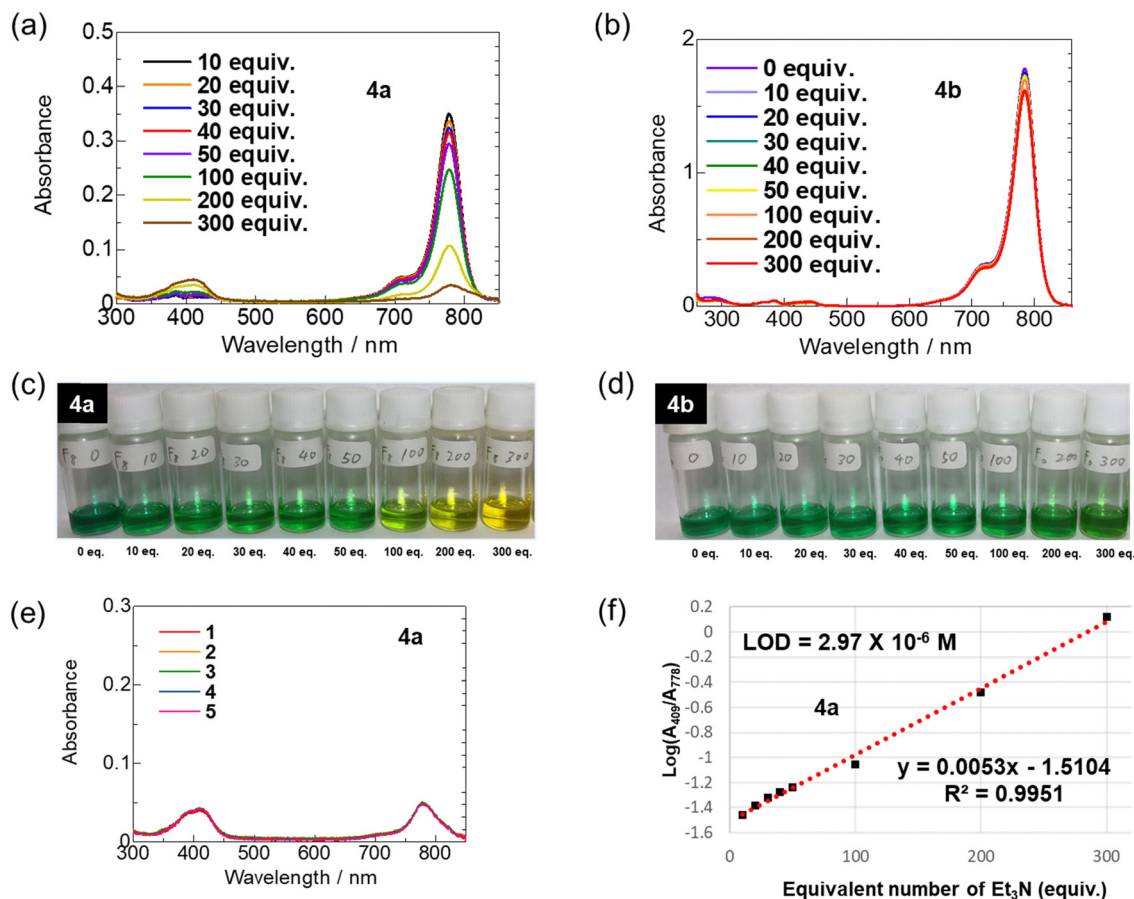

Fig. 9 Photostabilities of HMCDs **4a** and **4b** under white LED irradiation (8.5 W) in an incubator at 25 °C in CH$_2$Cl$_2$ solutions (1 × 10^{-6} M).

Fig. 10 UV-vis-NIR absorption spectra (a) and photographs (c) of ring-fluorinated HMCD **4a** (5×10^{-6} M) in the presence of various amounts of TEA in DCM and UV-vis-NIR absorption spectra after the solution is left at room temperature for 4 h (b). Photographs (d) of HMCD **4b** (5×10^{-6} M) in the presence of various amounts of TEA in DCM. Standard deviation obtained from five measurements of the UV-vis-NIR spectra of HMCD **4a** in the presence of 300 equiv. of TEA in DCM (1×10^{-5} M) after the solution is left at room temperature for 4 h (e). Linear relationship between the absorption logarithm (A_{409}/A_{778}) of HMCD **4a** (5×10^{-6} M) with the amount of TEA in DCM (f).

Table 4 Absorption maximum of HMCDs **4a** and **4b** in the presence of various amounts of TEA in DCM (5×10^{-6} M) after the solution was prepared and left at room temperature for 4 h

Dye	Equiv. of TEA	$\lambda_{abs}{}^{a}$ (nm)
4a	0	778
	10	778, 416
	20	778, 413
	30	778, 412
	40	778, 412
	50	778, 412
	100	778, 409
	200	782, 409
	300	409
4b	0	785
	10	784
	20	784
	30	784
	40	784
	50	784
	100	784
	200	784
	300	784

^{a} Measured in CH_2Cl_2 (5×10^{-6} M).

overnight and drying at room temperature overnight. The green colour of the filter paper adsorbing non-fluorinated HMCD **4b** did not change in the presence of TEA vapour (Fig. 12(b)). However, notably, when the blueish-green filter paper adsorbing ring-fluorinated HMCD **4a** was exposed to TEA or low-nucleophilicity ammonia vapour, the green filter paper responded within 1 s and showed a rapid and visible colour change from blueish-green to pale yellow (Fig. 12(a)). Non-fluorinated HMCD **4b** adsorbed on weakly acidic silica gel changed only slightly in response to NH_3 vapor,[10] whereas ring-fluorinated HMCD **4a** adsorbed on the neutral filter paper reacted quickly, even with low-nucleophilicity NH_3 vapour.

Exposure of ring-fluorinated HMCD **4a** adsorbed on the filter paper to the vapour of other primary amines, such as ethylamine, *n*-propylamine, and *n*-butylamine, and secondary amines, such as diethylamine, pyrrolidine, and piperidine, instantly causes the same vapochromic-responsive behaviour, along with a colour change from blue to green to pale yellow (Fig. 13(a) and (b)). No response is observed when ring-fluorinated HMCD **4a** adsorbed on the filter paper is exposed to an aromatic amine, such as aniline (Fig. 13(d)).
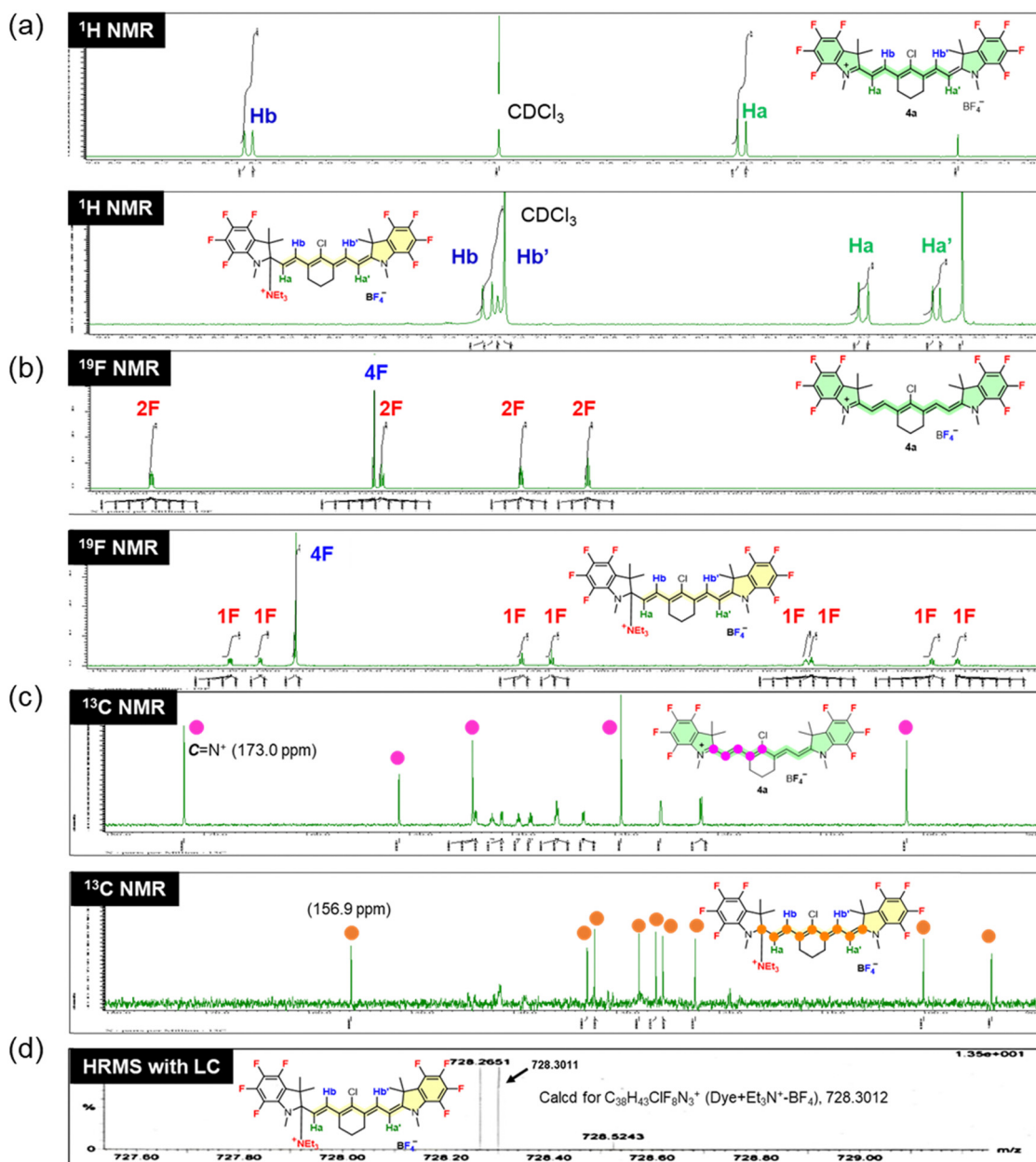
Fig. 11 ^{1}H NMR spectra (a), ^{19}F NMR spectra (b), and ^{13}C NMR spectra (c) of ring-fluorinated HMCD **4a** without or with an excess amount of TEA in CDCl$_3$ and HRMS results (d).

However, the colour of the filter paper adsorbing ring-fluorinated HMCD **4a** does not revert from pale yellow to blueish-green when left in air. However, ring-fluorinated HMCD **4a** adsorbed on the filter paper is reversibly converted to the original HMCD when exposed to HCl vapour, as shown in Fig. 13(a)–(c). Fig. 14 presents the results of the repeatability tests with NH$_3$ and HCl vapours on ring-fluorinated HMCD **4a** adsorbed on the filter paper. The filter paper adsorbing ring-fluorinated HMCD **4a** exhibits excellent repeatability in terms of colour switching, which occurs 13 times.

The unique vapochromic-responsive phenomenon, along with the colour change towards various primary and secondary amines including ammonia, can be ascribed to the nucleophile addition into the iminium double bond of the aromatic ring-fluorinated HMCD (**4a**) on the filter paper, similar to that in the DCM or CDCl$_3$ solution.

Conclusions

The introduction of fluorine atoms into the aromatic ring of HMCDs reduced the HOMO and LUMO levels of the HMCDs. Consequently, various primary alcohols, despite being weakly neutral nucleophiles, were added to ring-fluorinated HMCD **4a** in an alcohol solvent, and the colour of the solution changed from green to yellow. This phenomenon was also observed
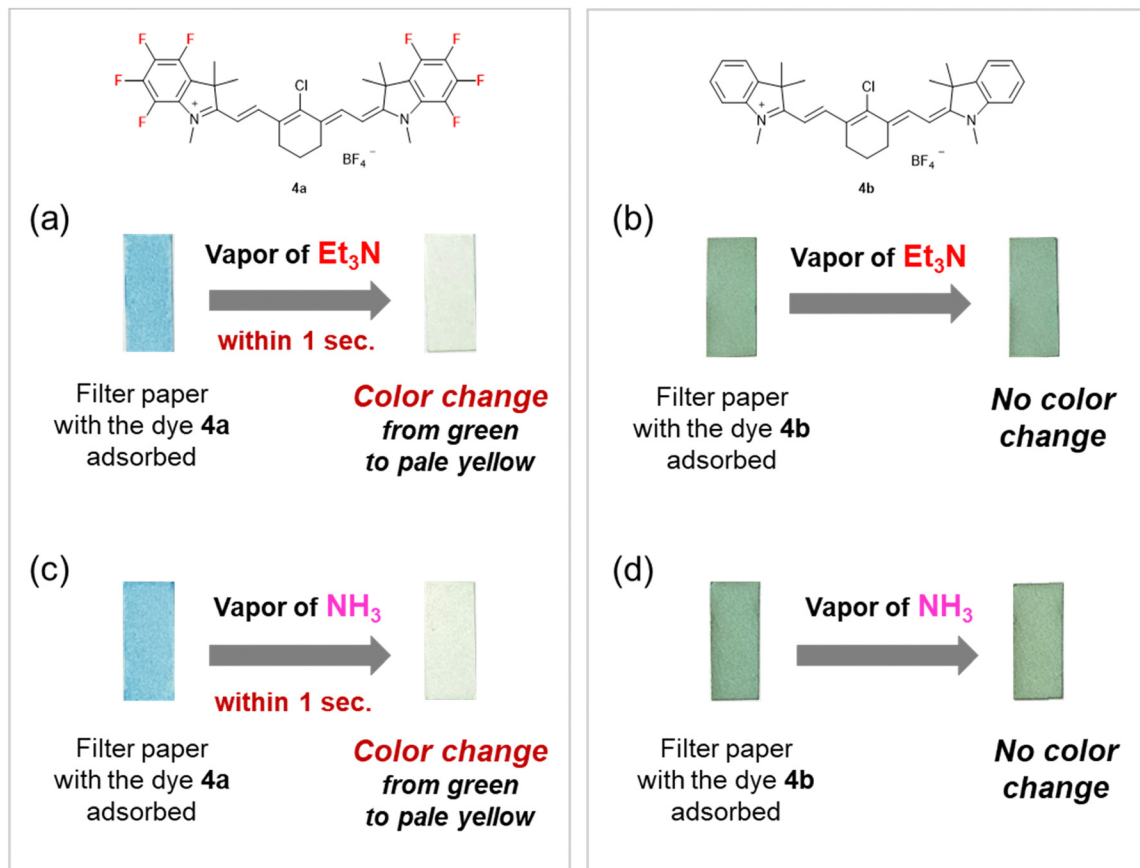
Fig. 12 Photographs of ring-fluorinated HMCD **4a** adsorbed on the filter paper with TEA vapour (a), HMCD **4b** adsorbed on the filter paper with TEA vapour (b), ring-fluorinated HMCD **4a** adsorbed on the filter paper with NH₃ vapour (c), and HMCD **4b** adsorbed on the filter paper with NH₃ vapour (d).
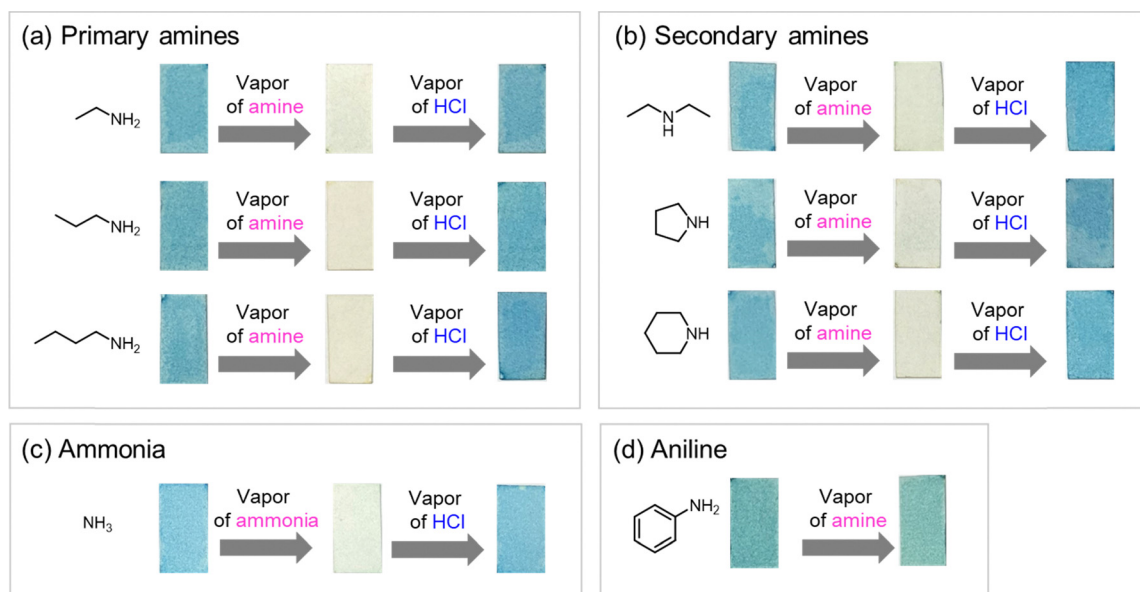
Fig. 13 Vapochromic discolouration and colouration test of ring-fluorinated HMCD **4a** adsorbed on the filter paper with various primary amines (a), secondary amines (b), and aniline (c).

when TEA was added to a DCM solution of ring-fluorinated HMCD **4a**. The addition of TEA to the iminium double bond of HMCD **4a** was confirmed by performing ^{1}H, ^{13}C, and ^{19}F NMR and HRMS on the solution. Based on the unique properties of

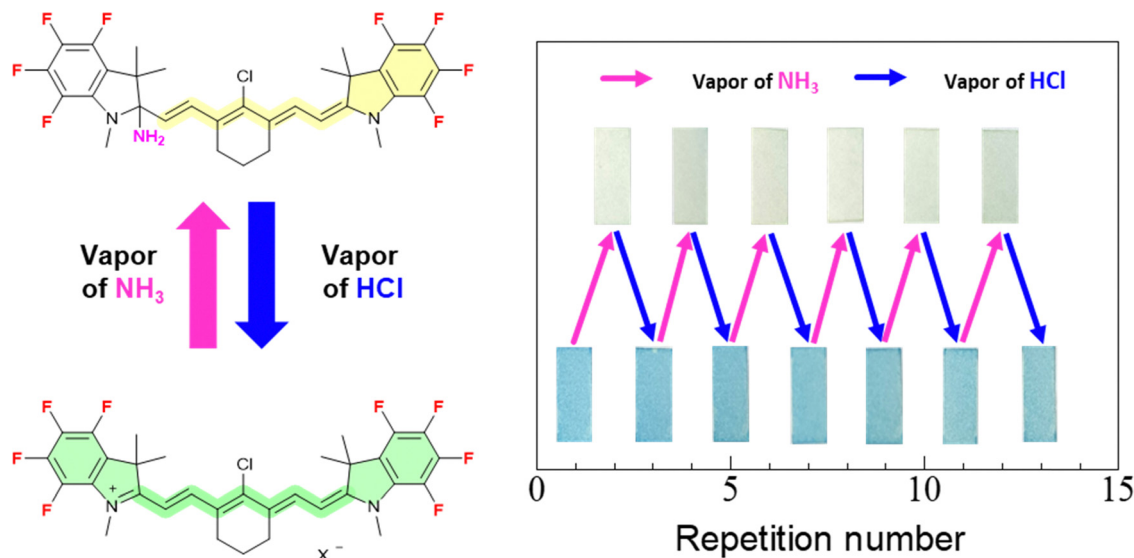**Fig. 14** Vapochromic discolouration and colouration repeatability test of ring-fluorinated HMCD **4a** adsorbed on the filter paper with NH$_3$ and HCl vapours.

ring-fluorinated HMCD **4a**, for the first time, we developed an HMCD adsorption filter paper, a near-infrared absorbent exhibiting reversible vapochromic response to weakly nucleophilic ammonia. These results are the first examples of intermolecular addition of weakly neutral nucleophiles into HMCDs and stimulus responsiveness not in solutions.

Experimental

Measurements

^{1}H NMR spectra were recorded at 392 or 400 MHz in CDCl$_3$, hexadeuteroacetone ((CD$_3$)$_2$CO), and hexadeuterodimethyl sulfoxide ((CD$_3$)$_2$SO) solutions, with tetramethylsilane (Me$_4$Si) as an internal standard, using a JEOL ECS-400 or ECX-400P FT-NMR spectrometer. ^{13}C NMR spectra were obtained at 99 or 101 MHz in CDCl$_3$, (CD$_3$)$_2$CO, and (CD$_3$)$_2$SO solutions, with Me$_4$Si as an internal standard, using the JEOL ECS-400 or ECX-400P FT-NMR spectrometer. ^{19}F NMR spectra were recorded at 369 or 376 MHz in CDCl$_3$, (CD$_3$)$_2$CO, and (CD$_3$)$_2$SO solutions, with CFCl$_3$ as an external standard, using the JEOL ECS-400 or ECX-400P FT-NMR spectrometer. The data were reported as s = singlet, d = doublet, t = triplet, q = quartet, quint = quintet, m = multiplet, br s = broad singlet, coupling constant(s), and integration. The melting points were determined using Yanagimoto MP-S3 micro-melting-point apparatus and were uncorrected. Electrospray ionisation mass spectroscopy in MeOH was performed using a JEOL JMS-T100LP instrument (Accu TOF LC-plus). UV-vis absorption spectra were recorded on Hitachi U-4100 and PerkinElmer Lamda950 instruments. Fluorescence spectra were recorded using a Jasco FP-8600 spectrofluorometer. The absolute fluorescence quantum yields were obtained using a HAMAMATSU Quantaurus-QY C11347-01 instrument. The fluorescence lifetimes were measured using a HAMAMATSU Quantaurus-Tau compact fluorescence lifetime spectrometer (C11367-01). Cyclic voltammetry was performed by employing an automatic polarisation system (HSV-110). TG-DTA was performed on an SII EXSTAR 6000 TG/DTA 6300 system under nitrogen after applying heat treatment at 100 °C under vacuum for 12 h, and the measured values were uncorrected. The X-ray crystal structure was evaluated using a Rigaku AFC 10 (CCD: Saturn 724 +) + VariMax Mo Optic system. 4,5,6,7-Tetrafluoro-2,3,3-trimethyl-3H-indole (**1**),[21] 1,2,3,3-tetramethyl-3H-indol-1-ium tetrafluoroborate (**2b**),[24] and (E)-2-chloro-3-(hydroxymethylene)cyclohex-1-enecarbaldehyde (**3**)[25] were prepared according to previously reported methods.

Synthesis

4,5,6,7-Tetrafluoro-1,2,3,3-tetramethyl-3H-indol-1-ium tetrafluoroborate (2a). A super-dehydrated chloroform (7.0 mL) solution of 4,5,6,7-tetrafluoro-2,3,3-trimethyl-3H-indol (0.324 g, 1.4 mmol) and trimethyloxonium tetrafluoroborate (0.419 g, 2.8 mmol) was stirred at 80 °C for 1 d. The reaction mixture was quenched with diethyl ether (100 mL × 3). The precipitate was purified via suction filtration to obtain 4,5,6,7-tetrafluoro-1,2,3,3-tetramethyl-3H-indol-1-ium tetrafluoroborate (0.392 g, 84%).

Yield 84%; m.p. 151–155 °C; R_f 0.65 (hexane/dichloromethane = 2/1); IR (KBr) 1523 (C=N) cm^{-1}; HRMS (ESI) found: m/z 246.0892; calcd for C$_{12}$H$_{12}$NF$_4$: M-BF$_4$, 246.0906; ^{1}H NMR (acetone-d_6) δ 1.70 (s, 6H, CH$_3$ × 2), 2.82 (s, 3H, CH$_3$), 4.13 (s, 3H, NCH$_3$); ^{13}C NMR (acetone-d_6) δ 14.2 (s), 20.7 (s), 38.7 (s), 57.2 (s), 125.6 (d, J = 18.7 Hz), 127.2 (s), 138.7 (dm, J = 256.9 Hz), 142.1 (dm, J = 255.4 Hz), 143.8 (dd, J = 250.2, 12.5 Hz), 200.6 (s); ^{19}F NMR (acetone-d_6) δ −155.7 (dd, J = 19.2, 3.0 Hz, 1F), −155.5 (td, J = 19.2, 3.0 Hz, 1F), −152.3 (tm, J = 18.1 Hz, 1F), −151.9 (s, 4F), −147.1 (tm, J = 18.1 Hz, 1F).

2-((E)-2-((E)-2-Chloro-3-(2-((E)-4,5,6,7-tetrafluoro-1,3,3-trimethylindolin-2-ylidene)ethylidene)cyclohex-1-en-1-yl)vinyl)-4,5,6,7-tetrafluoro-1,3,3-trimethyl-3H-indol-1-ium tetrafluoroborate (4a). A DMF (1.5 mL) solution of 4,5,6,7-tetrafluoro-1,2,3,3-tetramethyl-3H-indol-1-ium tetrafluoroborate (0.094 g, 0.3 mmol) and (E)-2-chloro-3-

Materials Advances

(hydroxymethylene)cyclohex-1-enecarbaldehyde (0.025 g, 0.15 mmol) was stirred at 23 °C for 18 h. The reaction mixture was cooled to room temperature, quenched with ice water (150 mL), filtered to remove the liquid, and concentrated under vacuum. The precipitate was purified by employing silica gel chromatography (dichloromethane/methanol = 20/1) to obtain 2-((E)-2-((E)-2-chloro-3-(2-((E)-4,5,6,7-tetrafluoro-1,3,3-trimethylindolin-2-ylidene)ethylidene)cyclohex-1-en-1-yl)vinyl)-4,5,6,7-tetrafluoro-1,3,3-trimethyl-3H-indol-1-ium tetrafluoroborate **4a** (0.089 g, 84%).

Yield 84%; T_{dt} 238.0 °C; R_f 0.43 (dichloromethane : methanol = 20 : 1); IR (KBr) 1558 (C=N) cm^{-1}; HRMS (ESI) found: m/z 627.1813; calcd for $C_{32}H_{28}ClF_8N_2$: M-BF$_4$, 627.1808; ^1H NMR (CDCl$_3$) δ 1.82 (s, 12H, CH$_3$ × 4), 1.89–1.92 (m, 2H, –CH$_2$CH$_2$CH$_2$–), 2.67 (t, J = 6.00 Hz, 4H, –CH$_2$CH$_2$CH$_2$–), 3.79 (s, 6H, NCH$_3$ × 2), 6.16 (d, J = 14.2 Hz, 2H, vinyl H), 8.30 (d, J = 14.2 Hz, 2H, vinyl H); ^{13}C NMR (CDCl$_3$) δ 20.6 (s), 26.4 (s, 2C), 34.6 (d, J = 9.3 Hz), 50.8 (s), 102.6 (s), 122.6 (d, J = 15.9 Hz), 126.6 (s), 130.4 (s), 135.4 (dd, J = 249.4, 13.2 Hz), 138.0 (dt, J = 252.3, 14.9 Hz), 141.7 (dt, J = 252.3, 14.9 Hz), 143.3 (dd, J = 249.4, 13.2 Hz), 144.9 (s), 152.0 (s), 173.0 (s); ^{19}F NMR (CDCl$_3$) δ −159.5 (t, J = 19.9 Hz, 2F), −157.5 (dd, J = 19.9, 14.2 Hz, 2F), −153.4 (tm, J = 19.9 Hz, 2F), −153.2 (s, 4F), −146.5 (dd, J = 19.9, 14.2 Hz, 2F).

2-((E)-2-((E)-2-Chloro-3-(2-((E)-1,3,3-trimethylindolin-2-ylidene)-ethylidene)cyclohex-1-en-1-yl)vinyl)-1,3,3-trimethyl-3H-indol-1-ium tetrafluoroborate (4b). A DMF (3.0 mL) solution of 1,2,3,3-tetramethyl-3H-indol-1-ium tetrafluoroborate (0.2658 g, 1.0 mmol) and (E)-2-chloro-3-(hydroxymethylene)cyclohex-1-enecarbaldehyde (0.088 g, 0.5 mmol) was stirred at 120 °C for 3 h. The reaction mixture was cooled to room temperature, quenched with ice water (150 mL), filtered to remove the liquid, and concentrated under vacuum. The precipitate was purified by performing silica gel chromatography (dichloromethane/methanol = 20/1) to obtain 2-((E)-2-((E)-2-chloro-3-(2-((E)-1,3,3-trimethylindolin-2-ylidene)ethylidene)cyclohex-1-en-1-yl)vinyl)-1,3,3-trimethyl-3H-indol-1-ium tetrafluoroborate (0.2226 g, 76%).

Yield 76%; T_{dt} 244.9 °C; R_f 0.43 (dichloromethane : methanol = 20 : 1); IR (KBr) 1551 (C=N) cm^{-1}; HRMS (ESI) found: m/z 483.2547; calcd for $C_{32}H_{36}ClN_2$: M-BF$_4$, 483.2562; ^1H NMR (acetone-d_6) δ 1.77 (s, 12H, CH$_3$ × 4), 1.91–1.97 (m, 2H, –CH$_2$CH$_2$CH$_2$–), 2.77 (t, J = 6.20 Hz, 4H, –CH$_2$CH$_2$CH$_2$–), 3.79 (s, 6H, NCH$_3$ × 2), 6.41 (d, J = 14.2 Hz, 2H, vinyl H), 7.32 (td, J = 7.3, 1.4 Hz, 2H, aryl H), 7.41–7.49 (m, 4H, aryl H), 7.62 (d, J = 7.3 Hz, 2H, aryl H), 8.44 (d, J = 14.20 Hz, 2H, vinyl H); ^{13}C NMR (acetone-d_6) δ 21.6 (s), 26.9 (s), 28.0 (s), 32.0 (s), 50.1 (s), 102.5 (s), 112.0 (s), 123.2 (s), 126.2 (s), 127.4 (s), 129.6 (s), 142.2 (s), 144.1 (s), 144.7 (s), 150.0 (s), 174.3 (s); ^{19}F NMR (acetone-d_6) δ −151.7 (s, 4F).

(E)-2-Chloro-3-(2-((E)-1,3,3-trimethylindolin-2-ylidene)ethylidene)cyclohex-1-ene-1-carbaldehyde (**5b**):[27] R_f 0.21 (hexane : dichloromethane = 1 : 2); IR (KBr) 1643 (C=O) cm^{-1}; ^1H NMR (chloroform-d) δ 1.66 (s, 6H, CH$_3$ ×2), 1.74–1.81 (m, 2H, -CH$_2$CH$_2$CH$_2$-), 2.48 (t, J = 5.84 Hz, 2H, -CH$_2$CH$_2$CH$_2$-), 2.58 (tm, J = 5.84 Hz, 2H, -CH$_2$CH$_2$CH$_2$-), 3.23 (s, 3H, -NCH$_3$), 5.46 (d, J = 12.8 Hz, 1H, vinyl H), 6.72 (d, J = 7.79 Hz, 1H, aryl H), 6.94 (tm, J = 7.79 Hz, 1H, aryl H), 7.19–7.24 (m, 2H, aryl H) 7.82 (d, J = 12.8 Hz, 1H, vinyl H), 10.3 (s, 1H, CHO); ^{13}C NMR (chloroform-d) δ 21.0 (s), 24.7 (s), 26.8 (s), 28.4 (s), 29.5 (s), 46.5 (s), 93.0 (s), 106.8 (s), 121.0 (s), 121.8 (s), 123.4 (s), 128.0 (s), 128.7 (s), 131.2 (s), 139.3 (s), 144.5 (s), 148.8 (s), 163.0 (s), 191.1 (s).

Preparation of the dye-adsorbed filter paper

The filter paper was dipped in a DCM solution (5×10^{-4} M) of the **4a** and **4b** dyes and allowed to stand in a refrigerator overnight to allow each dye to be adsorbed on the filter paper. After being removed and air-dried, the filter paper samples were exposed to the vapours of various amines.

Author contributions

SA performed the experiments on the synthesis and photophysical properties, analysed the data, and wrote part of the manuscript. TA and YU examined the single-crystal X-ray structure and analysed and summarised the data. YH performed the experiments on optical properties. YK and TI contributed useful discussions and comments on the synthesis, photophysical properties, and single-crystal X-ray structural analyses. KF conceived and designed the study and revised the manuscript.

Data availability

The data supporting this article have been included as part of the ESI.†

Conflicts of interest

There are no conflicts to declare.

Acknowledgements

References

1 For selected reviews, see. (a) Y. Zhang and Y. Jia, NIR-II Cyanine@albumin Fluorophore for Deep Tissue Imaging and Imaging-Guided Surgery, *SmartMat*, 2024, **5**, e1245; (b) X. Ma, Y. Huang, A. Li, X. Zeng, S. H. Liu, J. Yin and G.-F. Yang, The Aggregates of Near-Infrared Cyanine Dyes in Phototherapy, *ChemMedChem*, 2023, **18**, e202300204; (c) N. G. Medeiros, C. A. Braga, V. S. Câmara, R. C. Duarte and F. S. Rodembusch, *Asian J. Org. Chem.*, 2022, **11**, e202200095; (d) K. Ilina and M. Henary, Cyanine Dyes Containing Quinoline Moieties: History, Synthesis, Optical Properties, and Applications, *Chem. – Eur. J.*, 2021, **27**, 4230–4248; (e) R. M. Exner, F. Cortezon-Tamarit and S. I. Pascu, Explorations into the Effect of Meso-Substituents in Tricarbocyanine Dyes: A Path to Diverse Biomolecular Probes and Materials, *Angew. Chem., Int. Ed.*,

2021, **60**, 6230–6241; (*f*) L. Feng, W. Chen, X. Ma, S. H. Liu and J. Yin, Near-Infrared Heptamethine Cyanines (Cy7): from Structure, Property to Application, *Org. Biomol. Chem.*, 2020, **18**, 9385–9397; (*g*) A. Mishra, R. K. Behera, P. K. Behera, B. K. Mishra and G. B. Behera, Cyanines During the 1990s: A Review, *Chem. Rev.*, 2000, **100**, 1973–2012.

2 For selected recent reviews, see. (*a*) S. M. Usama and K. Burgess, Hows and Whys of Tumor-Seeking Dyes, *Acc. Chem. Res.*, 2021, **54**, 2121–2131; (*b*) S. Wang, B. Li and F. Zhang, Molecular Fluorophores for Deep-Tissue Bioimaging, *ACS Cent. Sci.*, 2020, **6**, 1302–1316; (*c*) B. Li, M. Zhao and F. Zhang, Rational Design of Near-Infrared-II Organic Molecular Dyes for Bioimaging and Biosensing, *ACS Mater. Lett.*, 2020, **2**, 905–917; (*d*) A. P. Gorka, R. R. Nani and M. J. Schnermann, Cyanine Polyene Reactivity: Scope and Biomedical Applications, *Org. Biomol. Chem.*, 2015, **13**, 7584–7598.

3 For a recent review, see. (*a*) P. J. Choi, T. I-H. Park, E. Cooper, M. Dragunow, W. A. Denny and J. Jose, Heptamethine Cyanine Dye Mediated Drug Delivery: Hype or Hope, *Bioconjugate Chem.*, 2020, **31**, 1724–1739; (*b*) M. M. Leitao, D. de Melo-Diogo, C. G. Alves, R. Lima-Sousa and I. J. Correia, Prototypic Heptamethine Cyanine Incorporating Nanomaterials for Cancer Phototheragnostic, *Adv. Healthcare Mater.*, 2020, **9**, 1901665; (*c*) Y. Zhang, A. C. Yen and Y. Zhao, Polymeric Nanocarriers Incorporating Near-Infrared Absorbing Agents for Potent Photothermal Therapy of Cancer, *Poly. J.*, 2016, **48**, 589–603. For recent examples, see. ; (*d*) A. St. Lorenz, E. R. Buabeng, O. Taratula and M. Henary, Near-Infrared Heptamethine Cyanine Dyes for Nanoparticle-Based Photoacoustic Imaging and Photothermal Therapy, *J. Med. Chem.*, 2021, **64**, 8798–8805; (*e*) H. Qian, Q. Cheng, Y. Tian, H. Dang, C. Teng and L. Yan, An Anti-Aggregation NIR-II Heptamethine-Cyanine Dye with a Stereo-Specific Cyanine for Imaging-Guided Photothermal Therapy, *J. Mater. Chem. B*, 2021, **9**, 2688–2696; (*f*) F. Wu, Y. Lu, X. Mu, Z. Chen, S. Liu, X. Zhou, S. Liu and Z. Li, Intriguing H-Aggregates of Heptamethine Cyanine for Imaging-Guided Photothermal Cancer Therapy, *ACS Appl. Mater. Interfaces*, 2020, **12**, 32388–32396; (*g*) X. Zhao, Z. Fan, Y. Qiao, Y. Chen, S. Wang, X. Yue, T. Shen, W. Liu, J. Yang, H. Gao, X. Zhan, L. Shang, Y. Yin, W. Zhao, D. Ding, R. Xi and M. Meng, AIEgens Conjugation Improves the Photothermal Efficacy and Near-Infrared Imaging of Heptamethine Cyanine IR-780, *ACS Appl. Mater. Interfaces*, 2020, **12**, 16114–16124; (*h*) S. Siriwibool, N. Kaekratoke, K. Chansaenpak, K. Siwawannapong, P. Panajapo, K. Sagarik, P. Noisa, R.-Y. Lai and A. Kamkaew, Near-Infrared Fluorescent pH Responsive Probe for Targeted Photodynamic Cancer Therapy, *Sci. Rep.*, 2020, **10**, 1283; (*i*) X. Mu, Y. Lu, F. Wu, Y. Wei, H. Ma, Y. Zhao, J. Sun, S. Liu, X. Zhou and Z. Li, Supramolecular Nanodiscs Self-Assembled from Non-Ionic Heptamethine Cyanine for Imaging-Guided Cancer Photothermal Therapy, *Adv. Mater.*, 2020, **32**, 1906711.

4 For examples of organic photovoltaics (OPV), see. (*a*) C. J. Traverse, M. Young, J. Suddard-Bangsund, T. Patrick, M. Bates, P. Chen, B. Wingate, S. Y. Lunt, A. Anctil and R. R. Lunt, Anions for Near-Infrared Selective Organic Salt Photovoltaics, *Sci. Rep.*, 2017, **7**, 16399; (*b*) J. Suddard-Bangsund, C. J. Traverse, M. Young, T. J. Patrick, Y. Zhao and R. R. Lunt, Organic Salts as a Route to Energy Level Control in Low Bandgap, High Open-Circuit Voltage Organic and Transparent Solar Cells that Approach the Excitonic Voltage Limit, *Adv. Energy Mater.*, 2016, **6**, 1501659; (*c*) Y. Zhao, G. A. Meek, B. G. Levine and R. R. Lunt, Near-Infrared Harvesting Transparent Luminescent Solar Concentrators, *Adv. Opt. Mater.*, 2014, **2**, 606–611; (*d*) H. Zhang, S. Jenatsch, J. De Jonghe, F. Nüesch, R. Steim, A. C. Véron and R. Hany, Transparent Organic Photodetector using a Near-Infrared Absorbing Cyanine Dye, *Sci. Rep.*, 2015, **5**, 9439; (*e*) A. C. Véron, H. Zhang, A. Linden, F. Nüesch, J. Heier, R. Hany and T. Geiger, NIR-Absorbing Heptamethine Dyes with Tailor-Made Counterions for Application in Light to Energy Conversion, *Org. Lett.*, 2014, **16**, 1044–1047; (*f*) H. Zhang, G. Wicht, C. Gretener, M. Nagel, F. Nüesch, Y. Romanyuk, J.-N. Tisserant and R. Hany, Semitransparent Organic Photovoltaics Using a Near-Infrared Absorbing Cyanine Dye, *Sol. Energy Mater. Sol. Cells*, 2013, **118**, 157–164; (*g*) P.-A. Bouit, D. Rauh, S. Neugebauer, J. L. Delgado, E. D. Piazza, S. Rigaut, O. Maury, C. Andraud, V. Dyakonov and N. A. Martin, Cyanine-Cyanine'' Salt Exhibiting Photovoltaic Properties, *Org. Lett.*, 2009, **11**, 4806–4809.

5 For examples of dye-sensitized solar cells (DSSC), see. (*a*) W. Naim, V. Novelli, I. Nikolinakos, N. Barbero, I. Dzeba, F. Grifoni, Y. Ren, T. Alnasser, A. Velardo, R. Borrelli, S. Haacke, S. M. Zakeeruddin, M. Graetzel, C. Barolo and F. Sauvage, Transparent and Colorless Dye-Sensitized Solar Cells Exceeding 75% Average Visible Transmittance, *JACS Au*, 2021, **1**, 409–426; (*b*) T. Geiger, I. Schoger, D. Rentsch, A. C. Veron, F. Ostwald, T. Meyer and F. Nuesch, Unsymmetrical Heptamethine Dyes for NIR Dye-Sensitized Solar Cells, *Int. J. Photoenergy*, 2014, 258984; (*c*) K. Funabiki, H. Mase, A. Hibino, N. Tanaka, N. Mizuhata, Y. Sakuragi, A. Nakashima, T. Yoshida, Y. Kubota and M. Matsui, Synthesis of a Novel Heptamethine-Cyanine Dye for Use in Near-Infrared Active Dye-Sensitized Solar Cells with Porous Zinc Oxide Prepared at Low Temperature, *Energy Environ. Sci.*, 2011, **4**, 2186–2192; (*d*) T. Ono, T. Yamaguchi and H. Arakawa, Study on Dye-Sensitized Solar Cell using Novel Infrared Dye, *Sol. Energy Mater. Sol. Cells*, 2009, **93**, 831–835; (*e*) A. Otsuka, K. Funabiki, N. Sugiyama, H. Mase, T. Yoshida, H. Minoura and M. Matsui, *Chem. Lett.*, 2008, **37**, 176–177; (*f*) M. Matsui, Y. Hashimoto, K. Funabiki, J.-Y. Jin, T. Yoshida and H. Minoura, *Synth. Met.*, 2005, **148**, 147–153.

6 For a cyanide anion, see. (*a*) L. Yijiang, Q. Dali, P. Hua, L. Mengnan, C. Hongbiao and L. Huaming, A Highly Selective Fluorescent Probe for Colorimetric Recognition of Cyanide Anion Based on Heptamethine

Cyanine-Triphenylamine Conjugate, *J. Photochem. Photobiol., A*, 2018, **364**, 151–158; (*b*) D. Qiu, Y. Liu, M. Li, H. Chen and H. Li, Near-Infrared Chemodosimetric Probes Based on Heptamethine Cyanine Dyes for the "Naked-Eye" Detection of Cyanide in Aqueous Media, *J. Lumin.*, 2017, **185**, 286–291; (*c*) Y. Wang, S.-Y. Gwon, Y.-A. Son and S.-H. Kim, Spectroscopic Characterization of Heptamethine Cyanine Dyes for the Interaction with the CN^- and F^-, *Mol. Cryst. Liq. Cryst.*, 2012, **566**, 61–66.

7 (*a*) A. Martin and P. Rivera-Fuentes, A general strategy to develop fluorogenic polymethine dyes for bioimaging, *Nat. Chem.*, 2024, **16**, 28–35; (*b*) A. Sakama, H. Seo, J. Hara, Y. Shindo, Y. Ikeda, K. Oka, D. Citterio and Y. Hiruta, Rational design of pH-responsive near-infrared spirocyclic cyanines: the effects of substituents and the external environment, *Chem. Commun.*, 2024, **60**, 5984–5987; (*c*) A. Mukherjee, P. C. Saha, R. S. Das, T. Bera and S. Guha, Acidic pH-Activatable Visible to Near-Infrared Switchable Ratiometric Fluorescent Probe for Live-Cell Lysosome Targeted Imaging, *ACS Sens.*, 2021, **6**, 2141–2146; (*d*) H. Mu, K. Miki, H. Harada, K. Tanaka, K. Nogita and K. Ohe, pH-Activatable Cyanine Dyes for Selective Tumor Imaging Using Near-Infrared Fluorescence and Photoacoustic Modalities, *ACS Sens.*, 2021, **6**, 123–129; (*e*) M. Oe, K. Miki and K. Ohe, An Enzyme-Triggered Turn-On Fluorescent Probe Based on Carboxylate-Induced Detachment of a Fluorescence Quencher, *Org. Biomol. Chem.*, 2020, **18**, 8620–8624; (*f*) M. Oe, K. Miki, H. Mu, H. Harada, A. Morinibu and K. Ohe, pH-Responsive Cy5 Dyes Having Nucleophilic Substituents for Molecular Imaging, *Tetrahedron Lett.*, 2018, **59**, 3317–3321; (*g*) H. Mu, K. Miki, Y. Takahashi, N. Teshima, M. Oe, K. Kojima and K. Ohe, pH Responsiveness of Near-Infrared Fluorescent Cyanine Dyes Encapsulated in Self-Assemblies Composed of Various Amphiphiles, *Chem. Lett.*, 2018, **47**, 1147–1150; (*h*) K. Miki, K. Kojima, K. Oride, H. Harada, A. Morinibu and K. Ohe, pH-Responsive Near-Infrared Fluorescent Cyanine Dyes for Molecular Imaging Based on pH Sensing, *Chem. Commun.*, 2017, **53**, 7792–7795; Other type of pH-responsive intramolecular addition at meso-position, see: (*i*) L. He, W. Lin, Q. Xu, M. Ren, H. Wei and J.-Y. Wang, A Simple and Effective "Capping" Approach to Readily Tune the Fluorescence of Near-Infrared Cyanines, *Chem. Sci.*, 2015, **6**, 4530–4536.

8 For reviews, see: F. Schüth, R. Palkovits, R. Schlögl and D. S. Su, *Energy Environ. Sci.*, 2012, **5**, 6278–6289; A. Klerke, C. H. Christensen, J. K. Nørskov and T. Vegge, *J. Mater. Chem.*, 2008, **18**, 2304–2310; For a recent example, see: Y. Ofuchi, K. Mitarai, S. Doi, K. Saegusa, M. Hayashi, H. Sampei, T. Higo, J. G. Seo and Y. Sekine, *Chem. Sci.*, DOI: **10.1039/D4SC04790G**.

9 For recent examples, see. (*a*) J. Wang, Z. Zhou, Y. Luo, T. Xu, L. Xu and X. Zhang, Machine Learning-Assisted Janus Colorimetric Face Mask for Breath Ammonia Analysis, *Anal. Chem.*, 2024, **96**, 381–387; (*b*) T. Zhou, J. Chen, T. Wang, H. Yan, Y. Xu, Y. Li and W. Sun, One-Dimensional Chain Viologen-Based Lanthanide Multistimulus-Responsive Materials with Photochromism, Photoluminescence, Photomagnetism, and Ammonia/Amine Vapor Sensing, *ACS Appl. Mater. Interfaces*, 2022, **14**, 57037–57046; (*c*) S. Yu, A. Tian, Q. Lu, X. Xu, S. Ma, X. Wang and Z. Wang, Polyoxometalate–Viologen Thermochromic Hybrids for Organic Amine Detectors and Memristors with Temperature-Regulating Resistance Switching Characteristics, *Inorg. Chem.*, 2023, **62**, 1549–1560; (*d*) I. Ahmad, A. A. Malik and A. A. Dar, Multi-Stimuli-Responsive Organo-Sulfonated Anil and Its Organic Complex, *Cryst. Growth Des.*, 2022, **22**, 6483–6492; (*e*) K. M. Fürpaß, L. M. Peschel, J. A. Schachner, S. M. Borisov, H. Krenn, F. Belaj and N. C. Mösch-Zanetti, Vapochromism and Magnetochemical Switching of a Nickel(II) Paddlewheel Complex by Reversible NH_3 Uptake and Release, *Angew. Chem., Int. Ed.*, 2021, **60**, 13401–13404; (*f*) X.-F. Wang, R.-L. Lin, W.-Q. Sun, J.-X. Liu, L.-X. Xu, C. Redshaw and X. Feng, Cucurbit[7]Uril-Based Self-Assembled Supramolecular Complex with Reversible Multistimuli-Responsive Chromic Behavior and Controllable Fluorescence, *Adv. Opt. Mater.*, 2024, **12**, 2400839; (*g*) X.-F. Wang, C.-Y. Xu, R.-L. Lin, W.-Q. Sun, M.-F. Ye, L.-X. Xu and J.-X. Liu, Acid–base regulated inclusion complexes of β-cyclodextrin with 1-[2-(4-fluorophenyl)-2-oxoethyl]-4,4-bipyridinium dichloride displaying multistimuli-responsive chromic behaviors and photomodulable fluorescence, *J. Mater. Chem. C*, 2024, **12**, 2764–2771; (*h*) S. Masuda, S. Kusumoto, M. Okamura, S. Hikichi, R. Tokunaga, S. Hayami, Y. Kim and Y. Koide, Thermosalient effect of a naphthalene diimide and tetrachlorocobaltate hybrid and changes of color and magnetic properties by ammonia vapor, *Dalton Trans.*, 2023, **52**, 10531–10536; (*i*) A. Rico, P. Le Poul, J. Rodríguez-López, S. Achelle and S. Gauthier, Exploring structural and optical properties of a new series of soft salts based on cyclometalated platinum complexes, *Dalton Trans.*, 2024, **53**, 11417–11425.

10 M. Shibayama, Y. Uehashi, S. Ajioka, Y. Kubota, T. Inuzuka and K. Funabiki, Vapochromism of Indolenine-based Heptamethine Cyanine Dye Adsorbed on Silica Gel, *New J. Chem.*, 2023, **47**, 5262–5269.

11 For recent examples, see. (*a*) S. Takahashi, M. Murai, Y. Hattori, S. Seki, T. Yanai and S. Yamaguchi, Sulfur-Bridged Cationic Diazulenomethenes: Formation of Charge-Segregated Assembly with High Charge-Carrier Mobility, *J. Am. Chem. Soc.*, 2024, **146**, 22642–22649; (*b*) W. Wu, K. Yan, Z. He, L. Zhang, Y. Dong, B. Wu, H. Liu, S. Wang and F. Zhang, *J. Am. Chem. Soc.*, 2024, **146**, 11570–11576; (*c*) M. Taki, K. Kajiwara, E. Yamaguchi, Y. Sato and S. Yamaguchi, Fused Thiophene-S,S-dioxide-Based Super-Photostable Fluorescent Marker for Lipid Droplets, *ACS Mater. Lett.*, 2021, **3**, 42–49; (*d*) S. Tian, H. Ma, X. Wang, A. Lv, H. Shi, Y. Geng, J. Li, F. Liang, Z.-M. Su, Z. An and W. Huang, Utilizing d–pπ Bonds for Ultralong Organic Phosphorescence, *Angew. Chem., Int. Ed.*, 2019, **58**, 6645–6649; (*e*) J. Yang, X. Zhen, B. Wang, X. Gao, Z. Ren, J. Wang, Y. Xie, J. Li, Q. Peng, K. Pu and Z. Li, The Influence

of the Molecular Packing on the Room Temperature Phosphorescence of Purely Organic Luminogens, *Nat. Commun.*, 2018, **9**, 840.

12 For recent examples, see. (*a*) K. Andoh, M. Murai, P.-A. Bouit, M. Hissler and S. Yamaguchi, Dithieno[3,2-b; 2',3'-f]phosphepinium-Based Near-Infrared Fluorophores: px–π* Conjugation Inherent to Seven-Membered Phosphacycles, *Angew. Chem., Int. Ed.*, 2024, **136**, e202410204; (*b*) N. Inai, S. Yamaguchi and T. Yanai, Theoretical Insight into the Effect of Phosphorus Oxygenation on Nonradiative Decays: Comparative Analysis of P-Bridged Stilbene Analogs, *ACS Phys. Chem. Au*, 2023, **3**, 540–552; (*c*) N. König, Y. Godínez-Loyola, H. Weiske, S. Naumov, P. Lönnecke, R. Tonner-Zech and C. A. Strassert, Evamarie Hey-Hawkins, Access to Strong Thieno[3,2-b]phosphole-Based Solid-State Emitters via Manganese(III)-Mediated Oxidative Annulation, *Chem. Mater.*, 2023, **35**, 8218–8228; (*d*) H. Ogasawara, Y. Tanaka, M. Taki and S. Yamaguchi, Late-Stage Functionalisation of Alkyne-Modified Phospha-Xanthene Dyes: Lysosomal Imaging Using an Off-On-Off Type of pH Probe, *Chem. Sci.*, 2021, **12**, 7902–7907; (*e*) M. A. Gonzalez, A. S. Walker, K. J. Cao, J. R. Lazzari-Dean, N. S. Settineri, E. J. Kong, R. H. Kramer and E. W. Miller, Voltage Imaging with a NIR-Absorbing Phosphine Oxide Rhodamine Voltage Reporter, *J. Am. Chem. Soc.*, 2021, **143**, 2304–2314; (*f*) M. Grzybowski, M. Taki, K. Kajiwara and S. Yamaguchi, Effects of Amino Group Substitution on the Photophysical Properties and Stability of Near-Infrared Fluorescent P-Rhodamines, *Chem. – Eur. J.*, 2020, **26**, 7912–7917.

13 For recent examples, see. (*a*) M. Murai, M. Abe, S. Ogi and S. Yamaguchi, Diazulenylmethyl Cations with a Silicon Bridge: A π-Extended Cationic Motif to Form J-Aggregates with Near-Infrared Absorption and Emission, *J. Am. Chem. Soc.*, 2022, **144**, 20385–20393; (*b*) J. B. Grimm, L. Xie, J. C. Casler, R. Patel, A. N. Tkachuk, N. Falco, H. Choi, J. Lippincott-Schwartz, T. A. Brown, B. S. Glick, Z. Liu and L. D. Lavis, A General Method to Improve Fluorophores Using Deuterated Auxochromes, *JACS Au*, 2021, **1**, 690–696; (*c*) T. Tsuda, S.-M. Choi and R. Shintani, Palladium-Catalyzed Synthesis of Dibenzosilepin Derivatives via 1,n-Palladium Migration Coupled with anti-Carbopalladation of Alkyne, *J. Am. Chem. Soc.*, 2021, **143**, 1641–1650; (*d*) N. B. Alexey, Modular Synthetic Approach to Silicon-Rhodamine Homologues and Analogues via Bis-aryllanthanum Reagents, *Org. Lett.*, 2021, **23**, 2604–2609; (*e*) A. S. Moses, O. R. Taratula, H. Lee, F. Luo, T. Grenz, T. Korzun, A. St. Lorenz, F. Y. Sabei, S. Bracha, A. W. G. Alani, O. D. Slayden and O. Taratula, Nanoparticle-Based Platform for Activatable Fluorescence Imaging and Photothermal Ablation of Endometriosis, *Small*, 2020, **16**, 1906936; (*f*) M. Pengshung, P. Neal, T. L. Atallah, J. Kwon, J. R. Caram, S. A. Lopez and E. M. Sletten, Silicon Incorporation in Polymethine Dyes, *Chem. Commun.*, 2020, **56**, 6110–6113.

14 (*a*) J. B. Grimm, A. N. Tkachuk, R. Patel, S. T. Hennigan, A. Gutu, P. Dong, V. Gandin, A. M. Osowski, K. L. Holland, Z. J. Liu, T. A. Brown and L. D. Lavis, Optimized Red-Absorbing Dyes for Imaging and Sensing, *J. Am. Chem. Soc.*, 2023, **145**, 23000–23013; (*b*) S. O. Oloo, G. Zhang,

P. Bobadova-Parvanova, S. Al Horani, M. Al Horani, F. R. Fronczek, K. M. Smith, M. da Graça and H. Vicente, Synthesis and Regioselective Functionalization of Tetrafluorobenzo-[α]-Fused BOPYPY Dyes, *Inorg. Chem.*, 2024, **63**, 9164–9174; (*c*) Y. Hayashi, N. Suzuki, T. Maeda, H. Fujiwara and S. Yagi, Photophysical Properties of 4-(5-Methylthiophen-2-yl)pyridiniumcyclic Enolate Betaine Dyes Tuned by Control of Twisted Intramolecular Transfer, *New J. Chem.*, 2021, **42**, 9770–9779; (*d*) T. D. Moseev, M. V. Varaksin, D. A. Gorlov, V. N. Charushin and O. N. Chupakhin, Transition-Metal-Free C-H/C-Li Coupling of Nonaromatic 2H-Imidazole 1-Oxides with Pentafluorophenyl Lithium in the Design of Novel Fluorophores with Intramolecular Charge Transfer Effect, *J. Org. Chem.*, 2020, **85**, 11124–11133; (*e*) K. Santra, I. Geraskin, M. Nilsen-Hamilton, G. A. Kraus and J. W. Petrich, Characterization of the Photophysical Behavior of DFHBI Derivatives: Fluorogenic Molecules that Illuminate the Spinach RNA Aptamer, *J. Phys. Chem. B*, 2019, **123**, 2536–2545; (*f*) R. III Chavez, L. Diodati, D. L. Wheeler, J. Shaw, A. L. Tomlinson and M. Jeffries-El, Evaluating the Impact of Fluorination on the Electro-optical Properties of Cross-Conjugated Benzobisoxazoles, *J. Phys. Chem. A*, 2019, **123**, 1343–1352.

15 For recent examples, see.(*a*) Y. Chang, Y.-S. Wu, S.-H. Tung, W.-C. Chen, C.-C. Chueh and C.-L. Liu, *ACS Appl. Mater. Interfaces*, 2023, **15**, 15745–15757; (*b*) K. Iguchi, T. Mikie, M. Saito, K. Komeyama, T. Seo, Y. Ie and I. Osaka, N-type Semiconducting Polymers Based on Dicyano Naphtho-bisthiadiazole: High Electron Mobility with Unfavorable Backbone Twist, *Chem. Mater.*, 2021, **33**, 2218–2228; (*c*) K. Ortstein, S. Hutsch, A. Hinderhofer, J. Vahland, M. Schwarze, S. Schellhammer, M. Hodas, T. Geiger, H. Kleemann, H. F. Bettinger, F. Schreiber, F. Ortmann and K. Leo, Energy Level Engineering in Organic Thin Films by Tailored Halogenation, *Adv. Funct. Mater.*, 2020, **30**, 2002987; (*d*) H. Wei, Y. Liu, Z. Liu, J. Guo, P.-A. Chen, X. Qiu, G. Dai, Y. Li, J. Yuan, L. Liao and Y. Hu, Effect of Backbone Fluorine and Chlorine Substitution on Charge-Transport Properties of Naphthalenediimide-Based Polymer, *Semiconductors, Adv. Electron. Mater.*, 2020, **6**, 1901241; (*e*) T. Hodsden, K. J. Thorley, J. Panidi, A. Basu, A. V. Marsh, H. Dai, A. J. P. White, C. Wang, W. Mitchell, F. Glöcklhofer, T. D. Anthopoulos and M. Heeney, Core Fluorination Enhances Solubility and Ambient Stability of an IDT-Based n-Type Semiconductor in Transistor Devices, *Adv. Funct. Mater.*, 2020, **30**, 2000325; (*f*) A. Y. Sosorev, V. A. Trukhanov, D. R. Maslennikov, O. V. Borshchev, R. A. Polyakov, M. S. Skorotetcky, N. M. Surin, M. S. Kazantsev, D. I. Dominskiy, V. A. Tafeenko, S. A. Ponomarenko and D. Y. Paraschuk, Fluorinated Thiophene-Phenylene Co-Oligomers for Optoelectronic Devices, *ACS Appl. Mater. Interfaces*, 2020, **12**, 9507–9519; (*g*) K. Yamamoto, S. Kato, H. Zajaczkowska, T. Marszalek, P. W. M. Blom and Y. Ie, Effects of Fluorine Substitution in Quinoidal Oligothiophenes for Use as Organic Semiconductors, *J. Mater. Chem. C*, 2020, **8**, 3580–3588.

16 For recent examples, see. (*a*) Z. Jia, S. Qin, L. Meng, Q. Ma, I. Angunawela, J. Zhang, X. Li, Y. He, W. Lai, N. Li, H. Ade,

C. J. Brabec and Y. Li, High performance tandem organic solar cells via a strongly infrared-absorbing narrow bandgap acceptor, *Nat. Commun.*, 2021, **12**, 178; (*b*) H. Ji, J. Li, M. Du, J. Yang, A. Tang, G. Li, Q. Guo and E. Zhou, Fluorination of the Quinoxaline-Based p-Type Polymer and n-Type Small Molecule for High VOC Organic Solar Cells, *J. Phys. Chem. C*, 2021, **125**, 10876–10882; (*c*) G.-U. Kim, C. Sun, J. S. Park, H. G. Lee, D. Lee, J.-W. Lee, H. J. Kim, S. Cho, Y.-H. Kim, S.-K. Kwon and B. J. Kim, Importance of Terminal Group Pairing of Polymer Donor and Small-Molecule Acceptor in Optimizing Blend Morphology and Voltage Loss of High-Performance Solar Cells, *Adv. Funct. Mater.*, 2021, **31**, 2100870; (*d*) Y. Firdaus, V. M. Le Corre, S. Karuthedath, W. Liu, A. Markina, W. Huang, S. Chattopadhyay, M. M. Nahid, M. I. Nugraha, Y. Lin, A. Seitkhan, A. Basu, W. Zhang, I. McCulloch, H. Ade, J. Labram, F. Laquai, D. Andrienko, L. J. A. Koster and T. D. Anthopoulos, Long-Range Exciton Diffusion in Molecular Non-Fullerene Acceptors, *Nat. Commun.*, 2020, **11**, 5220; (*e*) J. Yao, B. Qiu, Z.-G. Zhang, L. Xue, R. Wang, C. Zhang, S. Chen, Q. Zhou, C. Sun, C. Yang, M. Xiao, L. Meng and Y. Li, Cathode Engineering with Perylene-Diimide Interlayer Enabling over 17% Efficiency Single-Junction Organic Solar Cells, *Nat. Commun.*, 2020, **11**, 2726; (*f*) A. D. Fenta, S.-F. Liao, S.-W. Li, C.-F. Lu and C.-T. Chen, Increasing the Fluorine Substituent of Thieno[3,4-c]pyrrole-4,6-dione Terthiophene Copolymers Progressively Narrows the Nanofibrils and Enhances the Efficiency of Fullerene-Based Polymer Photovoltaics, *Macromolecules*, 2020, **53**, 7073–7083; (*g*) Q. Nie, A. Tang, P. Cong, L. Chen, Q. Zhang, H. Ji, G. Li, Q. Guo and E. Zhou, Wide Band Gap Photovoltaic Polymer Based on Pyrrolo[3,4-f]benzotriazole-5,7-dione (TzBI) with Ultrahigh VOC Beyond 1.25 V, *J. Phys. Chem. C*, 2020, **124**, 19492–19498; (*h*) P. Lei, B. Zhang, Y. Chen, Y. Geng, Q. Zeng, A. Tang and E. Zhou, Gradual Fluorination on the Phenyl Side Chains for Benzodithiophene-Based Linear Polymers to Improve the Photovoltaic Performance, *ACS Appl. Mater. Interfaces*, 2020, **12**, 38451–38459; (*i*) S. Wen, Y. Li, N. Zheng, I. O. Raji, C. Yang and X. Bao, High-efficiency organic solar cells enabled by halogenation of polymers based on 2D conjugated benzobis(thiazole), *J. Mater. Chem. A*, 2020, **8**, 13671–13678; (*j*) H. Jiang, X. Li, H. Wang, G. Huang, W. Chen, R. Zhang and R. Yang, Appropriate Molecular Interaction Enabling Perfect Balance Between Induced Crystallinity and Phase Separation for Efficient Photovoltaic Blends, *ACS Appl. Mater. Interfaces*, 2020, **12**, 26286–26292; (*k*) Y. Wang, H. Zhong, Y. Hong, T. Shan, K. Ding, L. Zhu, F. Liu, H. Wei, C. Yu and H. Zhong, Tailoring the Molecular Geometry of Polyfluoride Perylene Diimide Acceptors towards Efficient Organic Solar Cells, *J. Mater. Chem. C*, 2020, **8**, 8224–8233; (*l*) T. Liu, Y. Zhang, Y. Shao, R. Ma, Z. Luo, Y. Xiao, T. Yang, X. Lu, Z. Yuan, H. Yan, Y. Chen and Y. Li, Asymmetric Acceptors with Fluorine and Chlorine Substitution for Organic Solar Cells toward 16.83% Efficiency, *Adv. Funct. Mater.*, 2020, **30**, 2000456.

17 For recent examples, see. (*a*) R. Kani, Y. Miwa, Y. Kubota, T. Inuzuka, S. Kutsumizu and K. Funabiki, Rapid and Dual Optical CO$_2$-Responsive Polydimethylsiloxane Elastomer with Fluorinated Cyanine Dye, *Chem. – Asian J.*, 2023, **18**, e20230170; (*b*) R. Kani, Y. Kubota, T. Inuzuka and K. Funabiki, Aromatic Fluorine Atom-Induced Highly Amine-Sensitive Trimethine Cyanine Dye Showing Colorimetric and Ratiometric Fluorescence Change, *RSC Adv.*, 2022, **12**, 25587–25592.

18 P. Kirsch, *Modern Fluoroorganic Chemistry: Synthesis, Reactivity, Applications*, Wiley-VCH, Weinheim, 2013; K. Uneyama, *Organofluorine Chemistry*, Blackwell Pubs. Oxford, 2006; T. Hiyama, *Organofluorine Compounds: Chemistry and Applications*, Springer, Berlin, 2007.

19 (*a*) H. Ma, Y. Lu, Z. Huang, S. Long, J. Cao, Z. Zhang, X. Zhou, C. Shi, W. Sun, J. Du, J. Fan and X. Peng, ER-Targeting Cyanine Dye as an NIR Photoinducer to Efficiently Trigger Photoimmunogenic Cancer Cell Death, *J. Am. Chem. Soc.*, 2022, **144**, 3477–3486; (*b*) F. Niedermair, S. M. Borisov, G. Zenkl, O. T. Hofmann, H. Weber, R. Saf and I. Klimant, Tunable Phosphorescent NIR Oxygen Indicators Based on Mixed Benzo- and Naphthoporphyrin Complexes, *Inorg. Chem.*, 2010, **49**, 9333–9342.

20 (*a*) M. Henary and W. D. Wilson, *Carbocyanines for G-Quadruplex DNA Stabilization and Telomerase Inhibition*, WO2013012886 A1 2013-01-24; (*b*) M. E. Cooper, N. J. Gardner and P. G. Laughton, *Water Soluble Fluoro-Substituted Cyanine Dyes as Reactive Fluorescence Labelling Reagents*, WO2006111726 A1 2006-04-22.

21 (*a*) M. Eskandari, J. C. Roldao, J. Cerezo, B. Milian-Medina and J. Gierschner, Counterion-Mediated Crossing of the Cyanine Limit in Crystals and Fluid Solution: Bond Length Alternation and Spectral Broadening Unveiled by Quantum Chemistry, *J. Am. Chem. Soc.*, 2020, **142**, 2835–2843; (*b*) P. A. Bouit, C. Aronica, L. Toupet, B. Le Guennic, C. Andraud and O. Maury, Continuous Symmetry Breaking Induced by Ion Pairing Effect in Heptamethine Cyanine Dyes: Beyond the Cyanine Limit, *J. Am. Chem. Soc.*, 2010, **132**, 4328–4335; (*c*) W. Rettig and M. Dekhtyar, Merocyanines: Polyene-Polymethine Transition in Donor-Acceptor-Substituted Stilbenes and Polyenes, *Chem. Phys.*, 2003, **293**, 75–90; (*d*) L. M. Tolbert and X. Zhao, Beyond the Cyanine Limit: Peierls Distortion and Symmetry Collapse in a Polymethine Dye, *J. Am. Chem. Soc.*, 1997, **119**, 3253–3258.

22 https://www.olexsys.org/olex2/.

23 K. Funabiki, Y. Saito, T. Kikuchi, K. Yagi, Y. Kubota, T. Inuzuka, Y. Miwa, M. Yoshida, O. Sakurada and S. Kutsumizu, Aromatic Fluorine-Induced One-pot Synthesis of Ring-Perfluorinated Trimethine Cyanine Dye and Its Remarkable Fluorescence Properties, *J. Org. Chem.*, 2019, **84**, 4372–4380.

24 T. Zimmermann and O. Brede, 3H-Indolium Salts Efficiently Prepared from N-Substituted Anilines and α-Branched Ketones by An One-Pot Synthesis, *J. Heterocycl. Chem.*, 2004, **41**, 103–108.

25 J.-W. Yan, J.-Y. Zhu, K.-X. Zhou, J.-S. Wang, H.-Y. Tan, Z.-Y. Xu, S.-B. Chen, Y.-T. Lu, M.-C. Cui and L. Zhang, Neutral Merocyanine Dyes: for in vivo NIR Fluorescence Imaging of Amyloid-β Plaques, *Chem. Commun.*, 2017, **53**, 9910–9913.